



Theoretical Perspectives on Natural and Artificial Micro-swimmers

Jinan Liu¹ Yiqiang Fu¹ Xiongjun Liu² Haihui Ruan^{1*}

(¹Research Center for Fluid-Structure Interactions, Department of Mechanical Engineering, The Hong Kong Polytechnic University, Hung Hom, Kowloon, Hong Kong, China)

(²State Key Laboratory for Advanced Metals and Materials, University of Science and Technology Beijing, Beijing 100083, China)

Received 29 April 2021; revision received 26 July 2021; Accepted 2 August 2021;
published online 13 September 2021

© The Chinese Society of Theoretical and Applied Mechanics 2021

ABSTRACT The observations of microorganisms revealed how they swim. As inspired by them, studies on artificial micro-robots with various actuation mechanisms have been thriving. To elucidate the essential concepts in understanding the dynamic behaviors of natural and artificial micro-swimmers—so as to control the latter in future applications, in this paper, we summarize the historical achievements and describe our theoretical perspectives. We first introduce the studies on microorganisms and their propulsion mechanisms. After reviewing the basic principles and the development of the understanding of them, we take the flagellated micro-swimmers as an example to elaborate on the theories of their locomotion. We review the progress in actuation strategies of artificial flagellated micro-swimmers and then propose two possible strategies to realize the turning of a flagellated micro-swimmer—the key step toward steerability through remote fields. Finally, we describe the inadequacies of the investigations on this topic and our perspectives on future developments.

KEY WORDS Natural micro-swimmer, Artificial micro-swimmer, External field actuation, Manipulation strategies, Propulsion

1. Introduction

Richard Feynman delivered a forward-looking speech in 1959, in which he made the famous saying [1]. “It would be interesting in surgery if you could swallow the surgeon”. In 1966, the movie “Fantastic Voyage” pictured a small submarine entering a blood vessel to remove blood clots based on Feynman’s envision. The realization of this science fiction has become possible recently owing to the progress in the past few decades in micro-robotics [2]. In 2016, the Nobel Prize Committee in Chemistry awarded Jen Pierre Sauvage, Fraser Stoddart, and Ben Feringa in molecular machine design and synthesis, which exhibited the momentous development of this research field [3]. The past two decades also have witnessed a rapid progress of small robotic equipment, which benefited from the advance of micro-nanotechnology and smart materials [4]. These small-scale devices have shown great potential in medical cargo delivery [5–9] and water remediation [10–12].

Soft and small robots have drawn widespread attention owing to their increased flexibility and adaptability as compared to the hard and large ones. The motion of these robots is reminiscent of

* Corresponding author. E-mail: hhruan@polyu.edu.hk

that of natural micro-swimmers. Thus, a review of the biomechanics of microorganisms is essential to the inspiration of innovative artificial micro-swimmers because the development of the latter usually engages in finding a suitable propulsion and steering strategy [13]. In addition, an overview of the current achievements of artificial micro-swimmers and the corresponding propulsion strategies can foster further innovations. It is noteworthy that an efficient strategy can be a combination of two or even more different propulsion methods, for example, micro-swimmers may be driven by ultrasonic waves, but navigate and perform therapeutic functions in magnetic fields. In the last section of this article, the feasibility of such a mixed strategy will be explored based on a numerical model.

It is noted that there have been numerous review articles in the field of micro-swimmers. While the early articles summarized the studies of microorganisms, most of the recent ones focused on the actuation, manufacturing, and applications of artificial micro-swimmers. In 1976, James Lighthill's classic lecture [14] gave an overview of biofluid-dynamics of flagellated microorganisms. In 1996, Lighthill reviewed previous studies of swimming dynamics and then developed his classical theories to helical propulsion [15]. In 2009, Lauga concluded the hydrodynamics of microorganisms in his famous review article [16], wherein he discussed an example of applying the theories of natural micro-swimmers to artificial ones. After that, he further reviewed the developments of the theories for microorganisms in 2015 [17] and 2016 [18]. Compared with the reviews on natural micro-swimmers, the review articles on artificial micro-robots are much more abundant due to the rapid growth of this field. For example, the physics of microparticles was reviewed in Refs. [19, 20] because of their potential use for drug-delivery applications, micro-robots driven by chemical, acoustic and magnetic powers were reviewed in Refs. [21–28], and more actuation methods and their potential medical applications were reviewed in Refs. [3, 25, 29–32]. However, the aforementioned review articles seldom discuss the relation between the theories of microorganisms and the dynamics of micro-robots. In 2009, Abbott et al. [33] analyzed the suitable external powers for artificial micro-swimmers with their review beginning from the theories of microorganisms. After 12 years, as many artificial micro-swimmers have been synthesized and tested, we feel the need to review the studies on both natural and artificial micro-swimmers again and to see how the theories arising from the observation and abstraction of the former can assist the design and optimization of the latter.

In Sect. 2, we summarize some historical achievements and describe theoretical perspectives on natural micro-swimmers. We first introduce some studies on the propulsive mechanisms of microorganisms and review the basic principles and the development of the prehension of them. After that, we focus on micro-swimmers with oscillating flagella, i.e., flagellated micro-swimmers, and elaborate theoretically on the dynamic behaviors of their locomotion. The progress of artificial micro-swimmer is reviewed in Sect. 3, wherein various driving mechanisms, such as catalytic propulsion, magnetic power, and acoustic actuation, are briefly discussed. In Sect. 4, we propose two actuation strategies to realize the steering of a flagellated micro-swimmer by virtue of a bar-joint model method: the first one employs double acoustic sources to break the symmetry of periodic motion to make the micro-swimmer turn; the second combines the acoustic and magnetic power, where magnetic torques generated via magnetic nanoparticles inside the head of a flagellated micro-swimmer are responsible for navigation. The final section concludes the inadequacies of the existing investigations and our perspective on future developments.

2. Overview of Natural Micro-swimmers

2.1. Observations of Microorganisms

We define a “swimmer” as a creature or an object that moves by periodically changing its body configuration. This type of swimmer in nature, if the size is sufficiently small to be invisible to the naked eye, is usually called a microorganism. The biological observation of microorganisms began with the invention of the optical microscope in the seventeenth century when Anthony van Leeuwenhoek first observed swimming bacteria [34]. Since then, people have discovered that our world is full of swimming microorganisms like sperms, bacteria, protozoa, and algae.

In accordance with the comprehensive review article [16], many tiny swimmers use one or more appendages to advance. The appendage can be a rather hard spiral that can rotate. For example, the motor organelles of *Escherichia coli* and *Salmonella typhimurium* are bacterial flagella, which consist of a rotating motor, a spiral filament, and a hook that connects the motor to the filament [35–37].

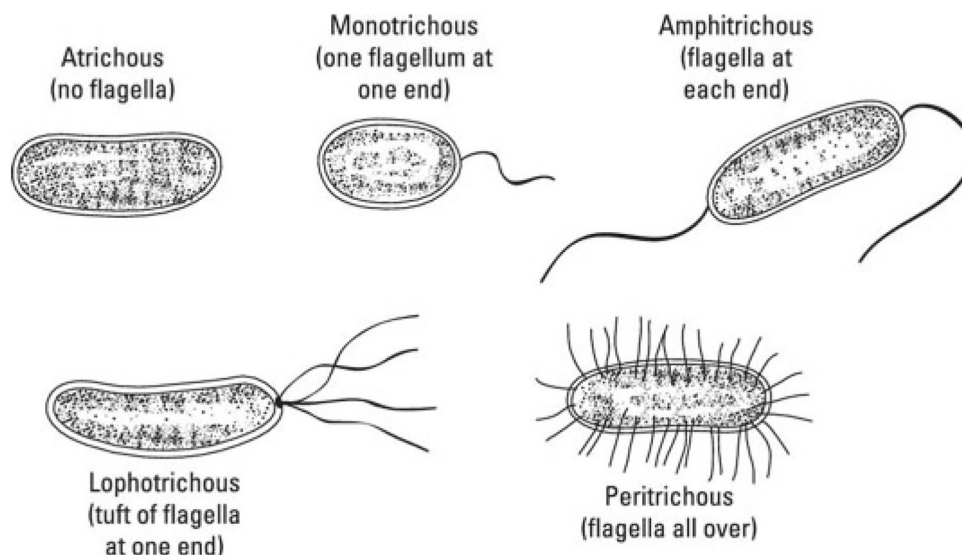


Fig. 1. Sketches of microscopic swimmers. Reproduced with permission [51]. Copyright 2019, Wiley

The diameter of the filament is around 20 nm with a 10- μm contour length of helix [38]. Each cell usually has several flagella. When the motor rotates counterclockwise, the filaments are wrapped in a bundle and the cell is pushed forward at a speed of 25–35 $\mu\text{m/s}$ [39]. When the motor runs clockwise, the corresponding filaments get unbundled and undergo a “polymorphic” transformation, in which the helix’s chirality changes; and these transformations can change the direction of cell movement [38]. Aside from the helical filament, the appendage can also be a flexible filament that undergoes whip-like motion driven by molecular motors, such as the sperms of many species [40].

As shown in Fig. 1, swimming bacteria have various flagellar configurations. For example, *F. crescentus* has a single right-handed spiral filament that is driven by a rotating motor and can be turned in any direction. The motor rotates clockwise preferentially and drives the filament to make the body move forward [41]. When rotating counterclockwise, the filament pulls the body instead of pushing it. The motor of *Rhodobacter sphaericus* only rotates in one direction, but it stops periodically [42]. The flagellar filaments form a tight coil prior to a stop and then extend into a spiral at a stop. Besides, a fraction of bacteria do not have flagella, they can also move slowly by the sliding [43].

Eukaryotic flagella and cilia are much larger than bacterial flagella, with a diameter of about 200 nm and a complex internal structure [40]. The most common structure has a molecular motor or dynein which slides back and forth causing fluctuations that propagate along the flagella. The beat pattern and length between eukaryotic flagella and cilia are very different. For example, *Chlamydomonas reinhardtii* have both cilia and flagella. Cilia are short and have random or non-synchronized motions [40], while flagella’s motion has a clear pattern. During the power stroke, each flagellum stretches and bends at the bottom, which is a bit reminiscent of the motion of our arms in breaststroke. During the recovery stroke, the flagella regain their folding, causing less resistance underneath.

Flagellated microorganisms, such as sperms, are more researched in the biomechanics community because of the simplicity—often involving only one flagellum for propulsion—and the large size which simplifies observation. One can notice two kinds of flagellar wave motions, helical and planar, and two corresponding trajectories of organisms. When the flagella move in a helical way, the overall trajectory is, in general, a straight line, though there exists helical rotation around the line [44–47]. It is interesting that in the case of planar flagellar motion, the trajectory turns out to be circular rather than linear [44, 46–49]. Further analysis demonstrates that the greater is the asymmetry of the flagellar wave motions, the smaller is the radius of curvature [47]. This indicates the existence of a strong connection between the circular path and the asymmetric tail beating [50]. However, more detailed interpretations of the results of biological observation are requisite, especially for biomimicking. This is the reason why

the investigations on the fundamental physics of natural micro-swimmers are emerging in an endless stream.

2.2. Swimming Mechanisms of Natural Micro-swimmers

2.2.1. Principles of Swimming on Microscale

The physics of microscopic swimming is distinct from the macroscopic one. The world of microorganisms is “a world with a very low Reynolds number (LRN)”, where inertia hardly plays a role and viscous damping is predominant. A general definition of the Reynolds number is $\text{Re} = \rho UL/\eta$, where ρ is the fluid density, η the dynamic viscosity, U and L the characteristic velocity and the length of the fluid, respectively. The specific Reynolds numbers for natural micro-swimmers are worth comparison [52]. In water, with fluid parameters $\rho \approx 1000 \text{ kg/m}^3$ and $\eta \approx 10^{-3} \text{ Pa}\cdot\text{s}$, a swimming bacterium, such as *E. coli*, with $U \approx 10 \text{ }\mu\text{m/s}$ and $L \approx 0.1 \text{ }\mu\text{m}$ is of a Reynolds number $\text{Re} \approx 10^{-5} - 10^{-4}$. A human sperm with $U \approx 200 \text{ }\mu\text{m/s}$ and $L \approx 50 \text{ }\mu\text{m}$ moves at $\text{Re} \approx 10^{-2}$. Some larger ciliates, such as *Paramecium*, with $U \approx 1 \text{ mm/s}$ and $L \approx 100 \text{ }\mu\text{m}$ can have $\text{Re} \approx 0.1$ [53]. Furthermore, for some much larger swimmers, such as fishes, birds, and insects, it is noted that their Reynolds numbers are usually very large, and thus, their swimming strategies will not work on a small scale [52, 54–58].

The study of the mechanisms of locomotion at LRNs has a long history. In 1930, Ludwig [59] remarked that microorganisms that swing their stiff arms like paddles cannot perform net movements. After that, there have been some classical reviews from different perspectives. Some were from the perspective of fluid mechanics at LRNs [53, 60–63]; some focused on the general animal locomotion [64]; and others found incentive from the investigations of the biophysics and biology of cell mobility [37, 65]. In general, one can simplify the sophisticated hydrodynamic problems at LRNs by studying the limit case $\text{Re} = 0$, in which the Navier–Stokes equations reduce to the Stokes equations [66]:

$$-\nabla p + \eta \nabla^2 \mathbf{u} = 0, \quad \nabla \cdot \mathbf{u} = 0 \quad (1)$$

where \mathbf{u} is the velocity field and p the fluid pressure. Since the Stokes equations, i.e., Eq. (1), are linear, the classical linear superposition method is practicable to solve the fluid field and pressure distribution. The Green’s function to Stokes flow $\mathbf{G}(\mathbf{x} - \mathbf{x}')$ can be solved analytically [67] and is expressed as:

$$\mathbf{G}(\mathbf{x} - \mathbf{x}') = \frac{1}{8\pi\eta} \left(\frac{\mathbf{I}}{r} + \frac{\mathbf{r}\mathbf{r}}{r^3} \right), \quad \mathbf{r} = \mathbf{x} - \mathbf{x}', \quad r = |\mathbf{r}| \quad (2)$$

where \mathbf{I} is the identity tensor. Physically, $\mathbf{G}(\mathbf{x} - \mathbf{x}')$ represents the velocity field at position \mathbf{x} due to a singularity force \mathbf{F} acting on the fluid domain at position \mathbf{x}' , and that is $\mathbf{u}(\mathbf{x} - \mathbf{x}') = \mathbf{G}(\mathbf{x} - \mathbf{x}') \cdot \mathbf{F}$ based on the linear superposition. Evidently, the flow velocity is inversely proportional to the spatial distance, allowing the neglect of the far-field effect.

A significant solution to Eq. (1) in terms of locomotion is denominated as directional anisotropy. For example, for a 2D problem, if there is a force $\mathbf{F} = (F, 0)$ exerted at $\mathbf{x}' = (r, 0)$, one can derive the flow field \mathbf{u} at $\mathbf{x} = (0, 0)$ as $(F/4\pi\eta r, 0)$ from Eq. (2); if $\mathbf{F} = (0, F)$, \mathbf{u} will then become $(0, F/8\pi\eta r)$. That is, for the same applied force, the flow velocity in the parallel direction is twice that in the perpendicular one ($u_{\parallel} = 2u_{\perp}$). Alternatively, in order to obtain the same speed, it is imperative to apply a force twice greater in the vertical direction than in the parallel direction ($F_{\perp} = 2F_{\parallel}$). In this case, one may note that the corresponding drag coefficients ξ_{\perp} and ξ_{\parallel} (the coefficient of proportionality between the local force and velocity) are different (typically $\xi_{\perp}/\xi_{\parallel} \approx 2$), i.e., the drag anisotropy. As we mentioned earlier, most biological swimmers apply elongated appendages, known as flagella, to swim. These slender filaments can intuitively remind us that the fundamental principle of swimming through resistance-based thrust is just the use of drag anisotropy at LRNs. To illustrate these ideas, we can take an undulating filament as an example, as depicted in Fig. 2. An infinitesimal element of the filament can be considered as rigid, and it moves at a speed of u which is at an angle of θ with regard to the whole filament. The horizontal component of the drag force f_{prop} , which propels the swimmer, is expressed as:

$$f_{\text{prop}} = (\xi_{\parallel} - \xi_{\perp}) u \sin \theta \cos \theta \quad (3)$$

With Eq. (3), only if the drag is anisotropic, e.g., $\xi_{\perp}/\xi_{\parallel} \approx 2$, there will be a net force in the propulsive direction. This resistance-based thrust theory is the so-called resistive force theory (RFT).

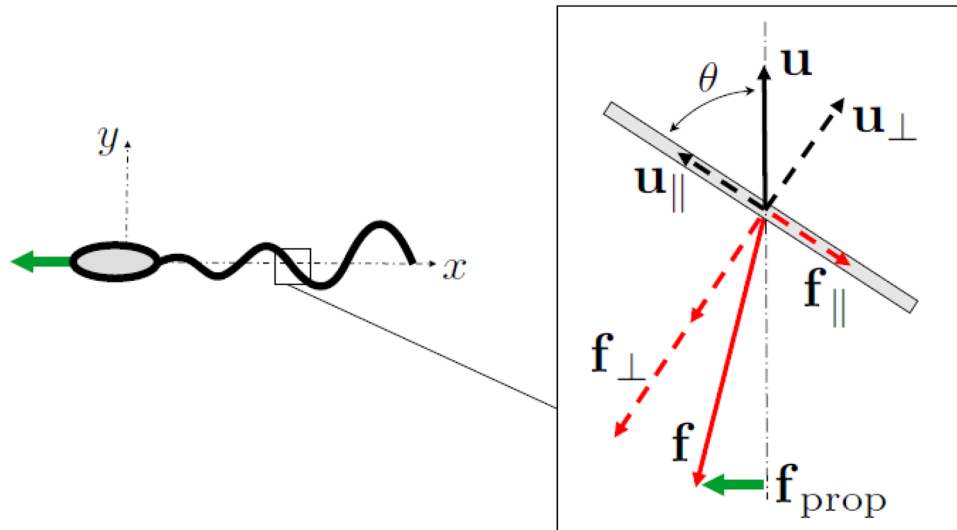


Fig. 2. Understanding of drag anisotropy for slender filaments. Reproduced with permission [16]. Copyright 2009, IOP Publishing

The feasibility of resistance-based thrust mainly depends on the following two important physical inferences: first, due to the existence of drag anisotropy, a micro-swimmer can generate propulsion in the direction perpendicular to the local movement direction of the filament; second, although the filament deforms reciprocally, it can still produce a nonzero time-averaged propulsive force [68, 69]. It should be accentuated that the periodic deformation of the filament needs to meet certain conditions to produce a nonzero time-averaged force as per Purcell's scallop theorem [62]. Purcell took scallops as an example for the explanation. Under LRNs, reciprocating motion cannot be used for movement; this is analogous to a scallop whose shell opens and closes alternatively while resulting in zero net displacement. Nevertheless, it is worth emphasizing that Purcell's scallop theorem is strictly valid only under the limited condition that all relevant Reynolds numbers in the swimming problem are zero. Many recent studies have been devoted to a more general issue by involving the inertia theorem (the Euler regime), and it has been found that the continuity of transition from the Stokerian regime to the Euler regime is normally dependent on the spatial symmetry of the problem [70–74].

2.3. Swimming Mechanisms

Gray and Hancock [68] and Lighthill [14] developed the aforementioned RFT to describe LRN swimming problems. This theory has been used to model the propulsion generated by spermatozoa [75], small earthworms [76], *Chlamydomonas reinhardtii* [77], and some swimmers in a granular material [78]. However, the drag coefficients were usually revised to better fit the observations rather than using the theoretical values given in Refs. [14, 68]. This theory has also been employed to interpret the propulsion mechanisms of helical flagella [77, 79–84] and nanobots [33, 85–87]. However, the RFT ignores the long-range hydrodynamic interaction and only regards the viscous force acting on the immersed body as a function of local velocity [88]. Thus, the slender body theory (SBT) [14, 89] and its advanced version, the regularized Stokeslet theory [90], have been proposed to improve the accuracy of modeling. Intuitively, applying the SBT to a micro-swimmer with an undulating flagellum (whose propulsion is usually estimated by the RFT) can be straightforward. According to the derivation of SBT [91], appropriate geometries of flagella require two properties: a small thickness-to-length ratio and a small displacement amplitude (compared with the wavelength) of the flagellum undulating. Fortunately, within an acceptable range, the predictions of SBT have shown great conformance with experimental observation [92] and the results of more complicated models established by the finite-element method [93], the regularized Stokeslet method [94], the boundary element method [95], *etc.* The equivalence between the SBT and the RFT has also been explored. For example, for helical flagella, the RFT was employed to express the forces and torques in terms of the translational and rotational

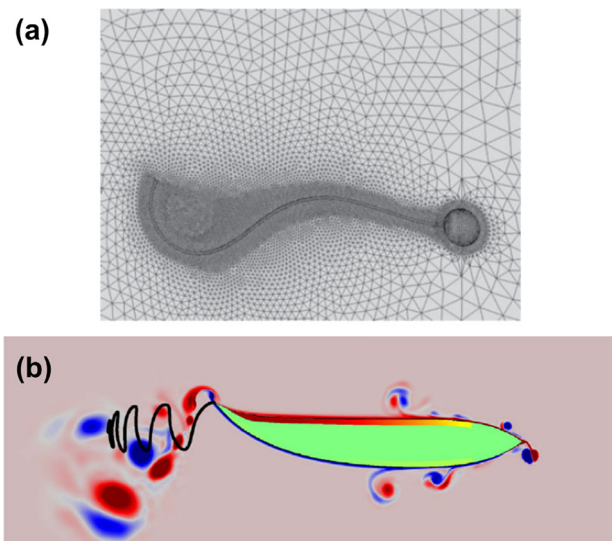


Fig. 3. Numerical simulations of natural swimmers: **a** finite-element mesh around the sperm-like swimmer. Reproduced with permission [88]. It is an open-access article that does not need to seek permission; **b** onset of vorticity of the fish-like swimmer. Reproduced with permission [99]. Copyright 2016, Elsevier

velocities [14, 68]. Reference [94] then experimentally examined the reliability of RFT and compared the experimental results with the theoretical predictions of the more involved SBT. All the theoretical predictions were in good accordance with experimental observations.

It is noted that these studies usually assumed idealized modeling conditions; for example, the filament model was assumed to be sufficiently slender, with a prescribed dynamic profile, and far from the boundary to satisfy the SBT. Subsequent research has mainly focused on the dynamics of swimmers close to the non-skid or free-skiing boundary adopting boundary element methods [96–98]. Rorai et al. [88] investigated the dynamics of a flagellated micro-swimmer, which is, more specifically, a sperm-like swimmer as demonstrated in Fig. 3a, in an infinite domain by finite element simulation, and an excellent agreement between the regularized Stokeslet method and the finite element simulation was demonstrated. However, their simulation did not consider a fully coupled fluid–structure interaction where the whole structure can have a rigid body motion, thus it became difficult to imitate the holistic locomotion of the swimmer. Curatolo et al. [99] proposed an approach to coupling the overall rigid body motion with the fluid–structure interaction for a fish-like swimmer by employing the automatic remeshing technique, as shown in Fig. 3b. However, they did not test the reliability of the RFT. Obviously, the geometry of the numerical model should be varied for a more comprehensive assessment of the analytical models, but the convergence of simulation can be a problem. Therefore, further research is needed to improve the numerical model of micro-swimmers through the fluid–structure interaction simulation.

According to the aforementioned Purcell’s scallop theorem [62], the breakthrough of the swimming problem for natural swimmers at LRNs is to find a non-reciprocal deformation approach. In 1951, Taylor found that a swimmer who deforms in a wave fashion can advance in an opposite direction to its traveling wave, and such a swimmer was named as Taylor’s swimming sheet thereafter [100]. Generally speaking, all the three-dimensional wave-like deformations can cause net propulsion, especially the spiral wave of flexible flagella [101]. It is noted that the original model of Taylor’s swimming sheet is infinitely long. Nevertheless, the Taylor sheet calculation is of great importance because it can be extended to finite objects. For example, to mimic the movement of ciliates such as opal and paramecium, Lighthill introduced an “envelope model”, where a traveling surface wave was exploited to simulate the swinging cilia embedded in the cell [102–104]. It is worth noting that the influence of inertia can be directly considered in the sheet calculation. In addition, it has been shown that if the flow separation is ignored, the swimming speed decreases with the increase of Reynolds number, and the asymptotic

value at high Reynolds number is half of Taylor's result [105, 106]. When the Reynolds number is zero and the waveform is prescribed, the nearby rigid wall, if exists, can increase the swimming speed if the gap between them is reduced [105].

2.3.1. Dynamic Behaviors of Flagellated Micro-swimmers

Inspired by Taylor's swimming sheet, one may have an intuitive understanding of the general problem of the self-propelled motion of flagellated swimmers at LRNs. For such micro-swimmers, their dynamic behaviors mainly arise from the interplay between the internal and external forces acting on them. Internal forces are normally from elastic properties and can resist the bending of flagella and ensure the inextensibility of their bodies, while external forces are mainly due to the fluid viscosity (which can be estimated from the RFT or the SBT) that can cause deformations of flagella and hence non-trivial dynamic behaviors. In an earlier study, Machin [107] found that the amplitude of the bending wave decayed exponentially with the length of a flagellum due to the fact that the LRN corresponds to overdamping. However, Machin scrutinized the fact that the swing amplitude of the sperm flagella did not attenuate but gradually increased with the distance from the head. Therefore, he concluded that in order to be consistent with experimental observations, there must be an internal actuation torque distribution along flagella, which turns out to be actin filaments afterward. Their study lays the foundation for many subsequent fluid-structure interaction problems at LRN [107–115] and has been further extended to the estimation of the actin filament's persistence length [116, 117]. Wiggins et al. [109] followed Machin's work and established the so-called hyper-diffusion equation with boundary conditions in terms of the normal drag coefficient ξ_{\perp} and the bending modulus EI for a flagellum with constant cross section, which is given by:

$$\begin{cases} \xi_{\perp} (\partial y / \partial t) = -EI (\partial^4 y / \partial x^4), 0 \leq x \leq L \\ \text{at } x = 0: y = y_0 \sin \omega t, y_x = \theta_0 \sin \omega t \\ \text{at } x = L: \partial^2 y / \partial x^2 = 0, \partial^3 y / \partial x^3 = 0 \end{cases} \quad (4)$$

where y is the transverse displacement of the flagellum with length L and is a function of time t and longitudinal coordinate x ; y_0 and θ_0 are the translational and rotational amplitudes of the wiggly head; and ω is the angular frequency. Equation (4) can be solved analytically by assuming y as the following:

$$y(x, t) = \sum_{n=1}^4 C_n e^{\lambda_n x} e^{-i\omega t} \quad (5)$$

where the four characteristic roots λ_n are determined by

$$\lambda_n = \sqrt[4]{\frac{i\omega\xi_{\perp}}{EI}}, \quad n = 1, 2, 3, 4 \quad (6)$$

It can be seen that Eq. (5) conforms to the above-mentioned Machin's solution [107], i.e., the fluctuation amplitude decays exponentially along the flagellum. Wiggins et al. [109] calculated the propulsive force by integrating the projected elastic force density along the flagellum because there was no other external force exerted on it. The expression of the normal elastic force f_e is:

$$f_e = EI (\partial^2 \kappa_e / \partial s^2 + \kappa_e^3 / 2) \quad (7)$$

where κ_e denotes the curvature of the flagellum at the arc coordinate s . By integrating f_e over the whole length L , the time-averaged propulsive force \bar{F} for the case of the translational boundary condition (i.e., $\theta_0 = 0$) is expressed as:

$$\bar{F} = \frac{1}{2} y_0^2 \xi_{\perp} \omega Y(S_p) \quad (8)$$

where Y is a function of the sperm number S_p and they are both dimensionless. The relation between Y and S_p is exhibited in Fig. 4. For the case of pivoting prosthesis (i.e., $y_0 = 0$), \bar{F} has a similar expression in terms of Y_p , which is also a function of the sperm number S_p as shown in Fig. 4. It is noted that based on Eq. (6), the real part of the characteristic root $\sqrt[4]{\omega\xi_{\perp}/EI}$ is of great significance and will influence the dynamic behavior of a sperm-like micro-swimmer. In fact, S_p is defined as $L\sqrt[4]{\omega\xi_{\perp}/EI}$, which

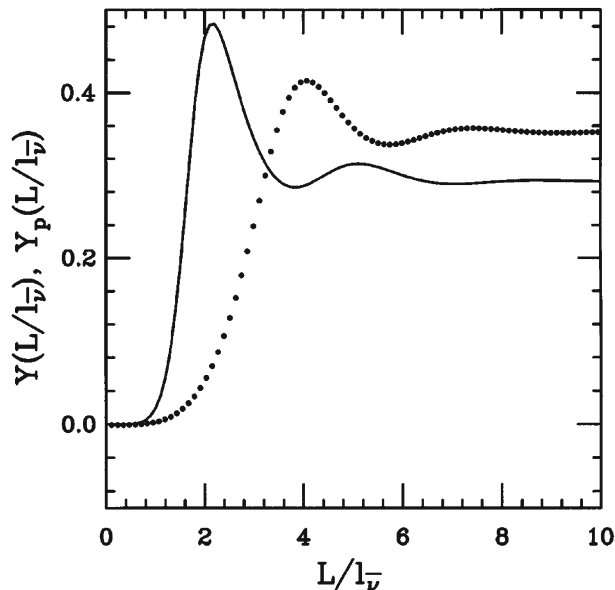


Fig. 4. Scaling functions Y and Y_p for propulsive force versus the sperm number S_p (which equals L/l_v). Dotted (Y) and solid lines (Y_p) indicate functions for the translational and pivoting prosthesis, respectively. Adapted with permission [109]. Copyright 1998, American Physical Society

is the most popular non-dimensional parameter used in micro-swimmer studies [107, 109, 118, 119] because it indicates the interplay between viscous and elastic forces on the flagellum.

In addition, the computed propulsive force based on the head movement has also been experimentally verified [112]. The propulsive force for a variable cross-section flagellum is proposed by Singh et al. [120]. One can first obtain the elastic force as:

$$f_e = EI\kappa_e^3 - EI(\partial^2\kappa_e/\partial s^2) - 2E(\partial I/\partial s)(\partial\kappa_e/\partial s) - E(\partial^2 I/\partial s^2)\kappa_e \quad (9)$$

where EI is a function of the arc length s . The propulsive force can then be estimated by integrating f_e . If the diameter of the cross section varies linearly, one can first derive the analytical solution of the equation of motion and then calculate the propulsive force by the RFT [119]. When such a micro-swimmer is placed in a fluid field, the effects of external forces, fluid viscous stresses, and internal bending moments can lead to complex dynamic deformations of the flagellum, which successively influences the swimming properties of the micro-swimmer. There have been many experimental and theoretical studies on the dynamics of such swimmers with regard to different sorts of microscale flows, such as extensional flows [121–123], vortex arrays [124–126], simple shear flow [127–132], pressure-driven channel flows [133], and other micro-fluidic flows [134, 135]. Some investigations have involved more complicated external or internal forces, such as forces at the ends of filaments [109, 136], two-body interactions [137], internal actuation [113, 138, 139], and self-attraction due to capillary interactions [140].

2.4. Summary of Natural Micro-swimmers

In this chapter, we have recapitulated the historical studies and theoretical perspectives on natural micro-swimmers such as sperms, bacteria, protozoa, and algae. They use one or more appendages to advance, which can be relatively hard spirals that can rotate or flexible filaments that undergo whip-like motion. The fundamental principle of swimming through resistance-based thrust is the use of drag anisotropy at LRNs. RFT, SBT, and finite element simulations have also been developed to address more details of hydrodynamics. In short, a periodic non-reciprocal deformation that can generate net propulsion arises from the interplay between the internal and external forces acting on each of the appendages, which has been clearly unveiled in modeling of flagellated micro-swimmers.

3. Overview of Artificial Micro-swimmers

3.1. Experimental Achievements of Artificial Micro-swimmers

3.1.1. Self-propulsion Approach

Artificial micro-swimmers or micro-robots swim in a low-Reynolds-number regime just like microorganisms, requiring swimming strategies that are distinct from those of macroscale swimmers. Researchers have proposed various propulsion mechanisms, many of which are biomimetic, to drive and control artificial micro-swimmers remotely. It is noted that some mechanisms are not biomimicking; however, as they can move microdevices in the fluid, the latter were also called micro-swimmers. In this sense, the concept of swimming has been expanded to describe all artificial microdevices propelled in the fluid. They are generally classified into three categories: self-propulsion, external propulsion, and a combination of them [30].

The foundation of self-propulsion approach is energy conversion. If there are local chemical reactions at the surface of a nano- or micro-swimmer, the chemical energy can be converted into kinetic energy. This energy transformation can eventually bring about the locomotion of artificial swimmers [22, 141–145]. The first fully artificial self-propelled nano-engine was synthesized by Paxton et al. [146] in 2004 and then followed by Fournier-Bidoz et al. [147]. Motivated by these achievements, some synthetic self-propelled micro-motors driven by catalytic reactions have been proposed [148–151]. While these autonomous swimmers can move at the speeds close to 1.5 cm/s, they are not steerable. As a result, the application of these self-propelled micro-swimmers normally limits to imprecise manipulations, which makes them incompetent for medical applications. To accurately control the movement of a swimmer, one may consider using field-propulsion rather than self-propulsion, and the field(s) can be magnetic, acoustic, photonic, thermal, or any combination of them [142, 152, 153].

3.1.2. Magnetic Actuation

The most renowned micro-robots actuated by rotating magnetic fields are helical swimmers [154, 155]. In 2007, Bell et al. [154] first reported a spiral-shaped magnetic swimmer that had a magnetic head and a spiral semiconductor tail made of a thin GaAs bilayer film as shown in Fig. 5a. This swimmer is an artificial duplicate of bacteria in terms of not only the dimensions but also the propulsion mechanism. Then, in 2012, Schuerle et al. reported a process to fabricate these magnetic swimmers by coating self-assembled phospholipidic helices with a magnetic CoNiReP alloy using electrodeless deposition [156]. After that, Gao et al. [157] developed a biotemplate technique to manufacture magnetic micro-robots through helical plant vessels in 2014. Recently, Nelson's team has proposed soft micro-swimmers composed of stimuli-responsive hydrogel bilayers [158–160], where the layer of poly-*N*-isopropylacrylamide (PolyNIPAM) is thermally responsive. The blending of magnetic nanoparticles and PolyNIPAM enables the hydrogel to move under magnetic manipulations. Moreover, by exploiting magnetic fields or near-infrared radiation, such magnetic nanoparticles can also generate heat, which is able to deform the temperature-sensitive PolyNIPAM layer. Magnetic nanoparticles can also be exploited to control the rolling direction of the hydrogel and produce magnetic shape anisotropy through appropriate design. These flexible micro-swimmers can adapt the surrounding environment and be actuated by rotating magnetic fields (direction changes with time), revealing the prospects in medical applications [160].

Another widely applied magnetic actuation method is the oscillating magnetic field (intensity changes with time) which is usually perpendicular to the trajectory of the swimmer. Dreyfus et al. [118] fabricated a magnetic micro-swimmer which had a flexible filament composed of DNA-linked chains of paramagnetic colloidal beads and investigated its behaviors under the actuation of oscillating magnetic field. Misra and co-workers demonstrated a sperm-like magnetic micro-swimmer composed of an ellipsoidal CoNi head and a soft flagellum made of SU-8 [161]. The on-off mechanism was also employed to actuate and control artificial micro-swimmers [162]. As shown in Fig. 5b, the repeated switch between “on” and “off” can generate a planar oscillating magnetic field. The basic driving principle of these micro-robots is based on the “dual-mass-spring system” which consists of four main components: a gold head, two nickel segments as the body, and a gold tail. These segments are connected by three springs, which are made of flexible silver, as demonstrated in Fig. 5b. When the magnetic field is “on”, the micro-swimmer is bent due to the magnetic forces on each segment. When “off”, the springs tend to restore the linkage to the original configuration. The transition during the “on/off” switching of the

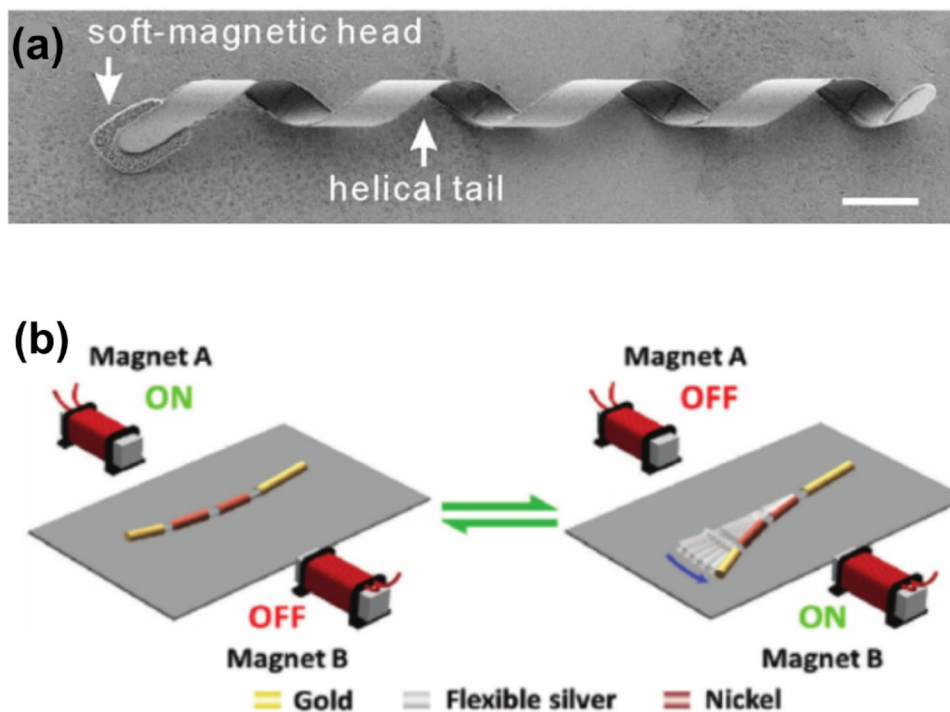


Fig. 5. Some examples of magnetic micro-swimmers: **a** artificial flagellum fabricated from a self-rolled semiconductor. Reproduced with permission [21]. Copyright 2009, AIP Publishing; **b** magnetic propulsion of an artificial nano-fish using a planar oscillating magnetic field. Reproduced with permission [162]. Copyright 2016, Wiley

magnetic field brings about various instant configurations. When the magnetic field oscillates near the resonant frequency of the swimmer, the dynamic response of the micro-swimmer can result in a net displacement.

3.1.3. Acoustic Actuation

Recently, acoustic actuation has been a considerably prevailing driving strategy for generating substantial propulsive force and has attracted much attention in terms of medical applications and lab-on-chip devices. Nevertheless, in consideration of its superb biocompatibility, the mechanisms of acoustic propulsion and precise manipulation deserve deep exploration.

As exhibited in Fig. 6a, some early acoustic artificial nano-swimmers are designed as geometrically asymmetric and composed of rigid metallic nano-rods [163], which can be suspended by an acoustic standing wave. Such an acoustic field, in which a series of nodes and antinodes are established from the bottom to the top, can be generated by the cooperation of a piezo-transducer and a reflector. These nodes are also the extreme points of the acoustic pressure of the standing wave. If the compressibility and the density of a nano-swimmer are greater than those of its surrounding fluid, the swimmer will be propelled toward the nodes. Wang et al. [163, 164] found that the metallic nano-rods could achieve a speed of around $200 \mu\text{m/s}$. Moreover, they discovered that these nano-rods exhibited striking interactions between nano-rods. The manipulation of an acoustic nano-swimmer was realized via incorporating Ni into the electrochemically grown nano-rods [165, 166], but it required to import an external magnetic field with a strength of 40–50 mT to steer the nano-rods, which was too strong to be implemented in bioapplications. Although acoustic-based artificial swimmers have been considered feasible in various medical circumstances, further studies are required to determine their driving mechanism and to predict their dynamic behaviors in biological environment.

Another type of acoustically propelled device employs the resonant behavior of microscale trapped bubbles within polyethylene-glycol-based cavities under acoustic actuation [167, 168]. The trapped bubble will oscillate if it is subject to a long-wavelength acoustic wave, especially when the wavelength

is much larger than the bubble diameter. Based on this principle, some micro-swimmers embedded with bubbles of different sizes have been designed to navigate under acoustic actuation [167, 168]. However, the controllability is poor due to the limitations of coupling between bubbles and the finite resonant-region [167]. Recently, Ahmed et al. developed a hybrid acousto-magnetic soft micro-robot [169]. As shown in Fig. 6b, their design includes an acoustic bubble at the center of the swimmer, and some superparamagnetic particles are carefully aligned along the length of the swimmer within a polymer matrix. Significant propulsive forces generated by these bubble-based swimmers are demonstrated, and the capability of swimming in viscous fluids makes practical applications more promising. However, the air bubbles can only remain stable for a few hours. Bubble-based swimmers for the next generation require more robust bubbles, and this may be achieved via polymeric coating technique.

We have mentioned in Sect. 2 that many microorganisms swim based on the flagellum, which could be a helix that rotates for propulsion or a flexible filament that wiggles for locomotion [16]. By mimicking the latter, Ahmed et al. [170] demonstrated the first flagellated artificial micro-swimmer propelled by acoustically actuated flagellum motion in 2016. They have shown that the flagellated micro-swimmer can be ten times faster than those propelled by acoustic streaming (i.e., without flagella). In the next year, as shown in Fig. 6c, Kaynak et al. [171] synthesized a larger sperm-like swimmer ($\sim 180 \times 60 \mu\text{m}$) that can achieve the terminal speed of 1.2 mm/s. These two experimental studies suggest that an artificial micro-swimmer with high motility must have one or several flagella; however, the mechanism of acoustic propulsion was not apparently elaborated therein. To comprehend it, Liu et al. [119] later proposed a driving mechanism based on head oscillation, which will be discussed in detail in Sect. 3.2.

3.1.4. Other Actuation Strategies

The possibility of employing optical and thermal energies for micro-swimmer actuation has also been explored. The first optically actuated micro-swimmer was fabricated by Jiang et al. [172], in which micro-swimmers were coated with a thin layer of Au onto silica hemispheres. This layer can absorb light and then generate a local temperature gradient which propels the micro-swimmers by thermophoresis. The further optical micro-swimmers exploit photocatalysis in which the propulsion arises from the light-induced catalytic reaction [173]. When the photocatalytic part of a micro-swimmer in a solution is illuminated, electron-hole pairs are generated by the photons. These holes and electrons are distributed on the surface of the photocatalytic material where they can react with the surrounding solution, and meanwhile, byproducts will be produced. This mechanism is similar to the conventional chemically catalytic propulsion strategy [22]. The collective behavior under light illumination has also been noted. For example, Ibele et al. demonstrated the collective behavior of micro-sized AgCl particles exposed to ultraviolet light in deionized water [174, 175].

Due to the difficulty of heat transfer, the strategy of heat-actuated micro- or nano-motors has seldom been reported. One possible way of employing heat to propel micro-swimmers is to incorporate an array of micro-heaters, which has been used in the study of a micro-swimmer consisting of shape memory alloy (SMA) components. During heating, the deformation of SMA parts can actuate the micro-robot [176–178]. The attempt of propelling micro-objects, such as bubbles and droplets, by the temperature gradient technique has also been reported [179, 180].

In general, combinations of some of the aforementioned methods may enhance the propulsion and manipulation of small-scale swimmers. Sitti and Schmidt et al. have recently proposed the application of bioengineered and biohybrid bacteria in drug delivery systems [181, 182]. We can also find several realizations of micro-swimmers that use magnetic power for control purposes (rather than for propulsion), for example, the micromotors that are self-driven in hydrogen peroxide (H_2O_2) solutions but magnetically navigated [183, 184]. Our study shown in Sect. 4 can be another example of the combination of acoustic and magnetic strategies.

We have introduced many actuation strategies so far. To have a comparison of them, the representative references are summarized in Table 1. One may notice that the characteristic velocities and dimensions vary remarkably from one actuation mechanism to another. Among them, acoustic bubble oscillation provides the highest speed, but the micro-swimmers propelled through acoustic flagellum whipping probably have the most balanced combination of speed, dimension, and easiness of manufacturing.

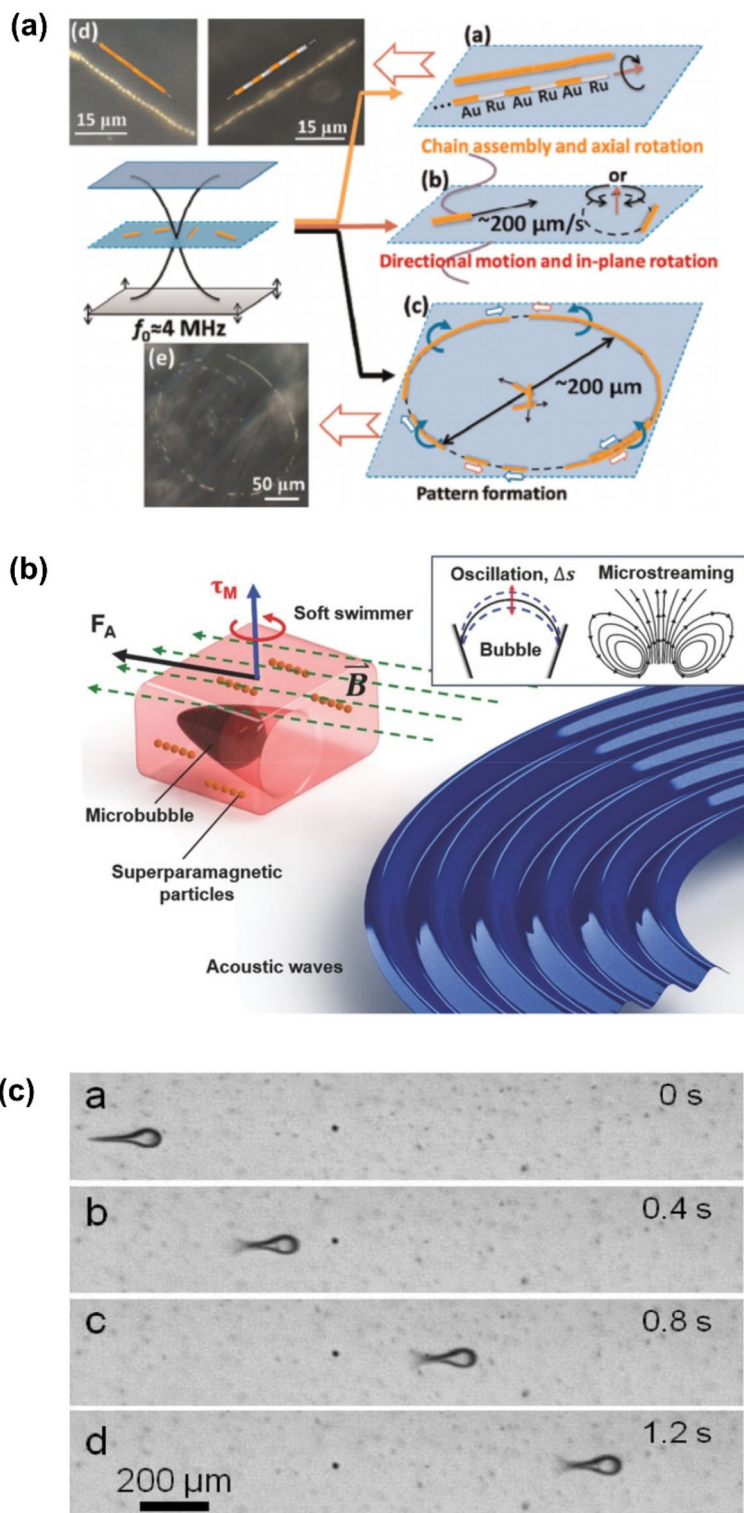
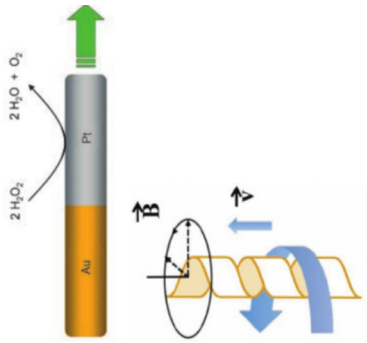
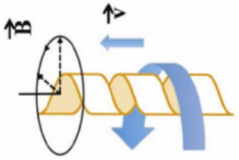
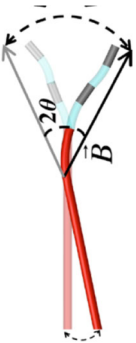
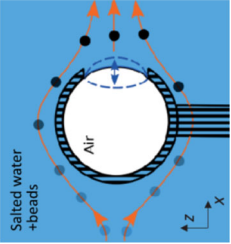


Fig. 6. Some examples of acoustic micro-swimmers: **a** schematics of the experimental setup and the acoustic propulsion of the nano-rods. Reproduced with permission [163]. Copyright 2012, American Chemical Society, **b** schematic illustrates the swimming mechanism of the acousto-magnetic soft micro-robot. Reproduced with permission [169]. Copyright 2017, Wiley, **c** the experimental observation of flagellated micro-swimmers' directional movement. Reproduced with permission [171]. Copyright 2017, Royal Society of Chemistry

Table 1. Comparison of different actuation mechanisms

Actuation mechanism	Representative sketch	Characteristic velocity ($\mu\text{m/s}$)	Characteristic dimension (μm)	References
Self-electrophoresis		5	2×0.4	[148]
Magnetically actuated helical rotation		0.5	10×2	[156]
Magnetically actuated flagellum whipping		10	15×0.1	[185]
Acoustic bubble oscillation		10,000	$50 \times \text{R10}$	[186]

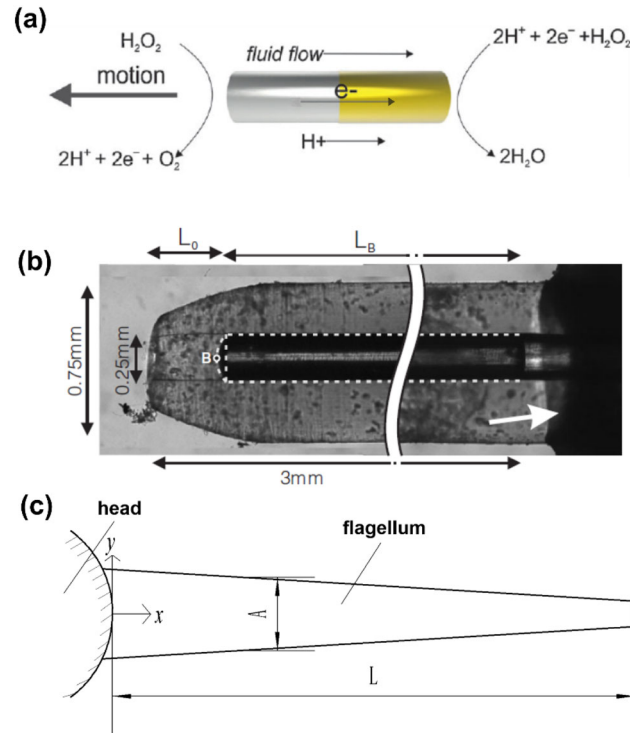


Fig. 7. Three examples of theoretical studies of artificial micro-swimmers: **a** schematic of motion of a Pt–Au nano-rod driven by the catalytic decomposition of hydrogen peroxide. Reproduced with permission [22]. Copyright 2015, Wiley; **b** a detailed image of an acoustic bubble actuator with the middle part removed, and the dark cylinder in the tube being the air bubble. Reproduced with permission [190]. Copyright 2006, IOP Publishing; **c** the idealized model of a sperm-like artificial micro-swimmer. Reproduced with permission [119]. Copyright 2020, IOP Publishing

3.2. Theoretical Studies of Artificial Micro-swimmers

Most of the basic mechanisms of propulsion strategies have been reviewed in the above context. In this section, we briefly emphasize the theoretical foundation of different propulsion strategies.

Micro-swimmers with bubbles have been widely studied. It has been unveiled that the driving forces, arising from the bubble oscillation, can be induced by H_2O_2 decomposition. The bubble-based micro-swimmer introduced in [147] has a nickel segment acting as the catalyst for H_2O_2 decomposition, i.e.,



Alternatively, if the O_2 gas generated based on Eq. (10) can be forced to flow along a prescribed direction, a micro-swimmer can also be propelled. This is the case of Pt–Au bimetallic nano-rods [149], as demonstrated in Fig. 7a, which utilizes the difference in the catalytic effects of these two metals. On the Pt surface, oxidation occurs and O_2 is produced. The electrons flow along the metallic nano-rod toward the Au side where reduction occurs. In this case, O_2 is pushed toward the Au side because of the proton gradient (H^+ ions are produced on the Pt side and consumed on the Au side), and the bimetallic nano-rod moves in the opposite direction.

Magnetic power is one of the most often employed propulsive strategies for artificial micro-swimmers due in large part to its prospect of remote and wireless operation, directional movement, and biocompatibility. In a magnetic field \mathbf{B} , a permanent magnet or a magnetic dipole with the magnetization of \mathbf{m} is subjected to a magnetic torque τ , which is the cross product of \mathbf{m} and \mathbf{B} , expressed as [187, 188]:

$$\tau = \mathbf{m} \times \mathbf{B} \quad (11a)$$

If the magnetic gradient $\nabla \mathbf{B}$ is nonzero, the magnet \mathbf{m} is subjected to a magnetic force:

$$\mathbf{F}_m = (\mathbf{m} \cdot \nabla) \mathbf{B} \quad (11b)$$

This is the reason why either a non-uniform or an oscillating magnetic field is applied to propel a magnetic micro-swimmer.

As for the acoustically actuated artificial micro-swimmers, the understanding of the driving mechanism behind the locomotion is still fragmented to date. A prevailing view regards the acoustic radiation force F_A as the streaming-induced Stokes drag subject to the micro-swimmer surface $\partial\Omega_1$, and the integral form is expressed as [170]:

$$F_A = \oint_{\partial\Omega_1} \langle \boldsymbol{\sigma}_2 \rangle \cdot \mathbf{n} dA - \oint_{\partial\Omega_1} \rho_1 \langle \mathbf{v}_1 \mathbf{v}_2 \rangle \cdot \mathbf{n} dA \quad (12)$$

where \mathbf{v}_1 and \mathbf{v}_2 are the vibration velocity of a micro-swimmer and the corresponding streaming velocity, respectively. The velocity field can be solved by the perturbation expansion approach [170, 189]. The bracket $\langle \rangle$ denotes the time-averaging within an acoustic period. The stress, $\boldsymbol{\sigma}_2$, is interlinked to \mathbf{v}_2 . The first term in Eq. (12) arises from the acoustic microstreaming and the second is due to the structural vibration of the micro-swimmer. However, in most cases, Eq. (12) cannot be straightforwardly used to solve the swimming problem. The finite element simulation is helpful, but it is often ill-conditioned due to the complex fluid–structure interaction circumstance.

Hence, more simplified models for theoretical calculation are in need for acoustic actuation. It is noted that the structure resonance of a micro-swimmer [related to the second term of Eq. (12)] may play an important role in propulsion. For a bubble-based acoustic micro-swimmer, as shown in Fig. 7b [190], the theoretical resonant frequency f_0 of the gas bubble can be estimated by [191]

$$f_0 = \frac{1}{2\pi} \sqrt{\frac{\kappa P_0}{\rho L_0 L_B}} \quad (13)$$

where κ is a frequency-dependent parameter related to the thermodynamic process, P_0 the initial pressure inside the bubble, ρ the fluid density, L_B the bubble length, and L_0 the length of a liquid column outside the bubble (Fig. 7b). If the surface tension effect is considered, a correction factor, which is in connection with the geometry of the bubble and the surface tension of the water–air interface, will be introduced into Eq. (13) [192]. The oscillation amplitude and the propulsive force can also be estimated at resonance [193].

For a flagellated micro-robot, e.g., a sperm-like artificial micro-swimmer, the dynamic behavior is more difficult to predict. Nevertheless, the review of natural microorganisms reminds us that we can convert this problem into a simple so-called hyper-diffusion problem [109], in which the drag force and the elastic force on the tail are balanced. Specifically, the simplification can bring about a partial differential equation (PDF) that governs the oscillation of a cantilever beam (the tail) which has oscillatory boundary conditions at its clamped end (the head), as depicted in Fig. 7c. The motion of the head can be determined by finite element simulations as demonstrated in Ref. [119], in which the Galerkin method [194–197] was employed to solve the PDF with the prescribed head motion (sinusoidal). It is noted that the inertia of the tail was not neglected in Ref. [119], which allows the study of the effect of resonance.

As we have mentioned, many artificial micro-swimmers are bioinspired. However, most studies only focus on the actuation strategies, fabrication processes, or experimental techniques, and the theoretical aspect (i.e., the principles of design and optimization) based on the swimming mechanisms at LRN is insufficiently addressed. Hence, as listed in Table 2, we categorized the references of natural and artificial micro-swimmers based on the types of propulsion mechanisms to remind the close relationship between them. Among them, the success in the theoretical description of microorganisms propelled by oscillating flagella [68, 77, 109, 198, 199] has inspired our preliminary work on artificial flagellated micro-swimmers described in the next chapter.

3.3. Summary of Artificial Micro-swimmers

In this chapter, the actuation methods of artificial micro-swimmers, classified into self-propulsion, external propulsion, and a combination of them, have been reviewed. A self-propulsion approach is generally based on local (electro)chemical reactions, e.g., H_2O_2 decomposition at the surface of a nano- or micro-swimmer, by which the chemical energy can be converted into kinetic energy. External propulsions may involve magnetic, acoustic, optical, and thermal fields. Magnetic power is most employed

Table 2. Categorized references of theoretical studies on propulsion mechanisms of microorganisms and their artificial counterparts

Propulsion mechanisms	References of natural micro-swimmers	References of artificial micro-swimmers
Helical filament	[35, 79–81, 83, 84, 94, 200–206]	[21, 157, 207–212]
Oscillating flagellum	[68, 77, 88, 107, 109, 120, 198, 199, 213]	[69, 75, 112, 118, 119, 170, 171, 211, 214, 215]
Cilia (multiple flagella)	[53, 85, 216–219]	[220, 221]
Propagation of kinks (without flagellum)	[222–224]	[162, 225]

because of its prospect of remote and wireless operation, directional movement, and biocompatibility. A magnetic micro-swimmer can be propelled via either a non-uniform or an oscillating magnetic field. Recently, acoustic actuation has been a considerably popular driving strategy because of its potential for medical applications and lab-on-chip devices. We have introduced acoustic micro-robots driven by acoustic standing waves, resonant trapped bubbles, microstreaming, and head oscillation, which can generate substantial propulsive forces. The employment of optical and thermal energies and combinations of some of the aforementioned methods for micro-swimmer actuation has also been introduced in this chapter.

4. Forward-Looking Strategies of Steering

In this section, let us shed some light on the possible strategies for steering a flagellated micro-swimmer propelled acoustically. We focus on this micro-swimmer because of the anticipation of its great potential in medical applications, considering the facts that ultrasound systems have been the most adopted clinical tools for diagnosis and therapy and a sperm-like structure is effortless to fabricate through 3D printing. It is noted that the governing equations for 2D flagellar dynamics are normally of significant nonlinearity due to the geometric nonlinearity of the flagellum and the influence of the rigid body motion. Besides, decoupling of the equations is generally difficult and may involve improper simplification and render convergence problems. Therefore, a discrete flagellum model is desired to solve the swimming problem. In 1976 [62], Purcell proposed a symmetric linkage with three links articulated at two hinges, known as Purcell’s three-link swimmer, which could be regarded as the “simplest animal” that could achieve locomotion at LRNs. Purcell demonstrated that this swimmer would be propelled along a straight line over one cycle of sequentially moving its front and rear bars. The dynamics of Purcell’s three-link swimmer has been further investigated since then [69, 226–229]. Inspired by Purcell’s three-link swimmer, using multi-link bars or bar-joint models, the dynamics of flexible flagella has been modeled. Alouges et al. [230] proposed a slender magnetoelastic swimmer, along which the magnetic-induced torques were distributed, and the governing equations of the elastic tail were reduced to a system of ordinary differential equations (ODEs). Their group has also investigated the optimal stroke of a multi-link swimmer based on the criterion of optimal energy efficiency [231]. Moreau et al. [232] compared the classical elasto-hydrodynamic formulation with the bar-joint model via the coarse-graining formalism and demonstrated that the latter could achieve better numerical performance.

Following the above methodology, a bar-joint model of a flagellum, which is equivalent to a linear discretization of a continuous beam, is employed. As shown in Fig. 8, a flexible flagellum can be discretized into multiple segments which are considered as straight and rigid bars. The joint between two bars has the property of a spring hinge and can provide the restoring moment. This kind of bar-joint model can easily be validated by comparing its solutions with those of the beam theory in terms of static deformation or vibration. Note that this model intrinsically fulfills the inextensibility constraints of a flexible tail without the introduction of the Lagrange multiplier [17, 233]. The RFT is employed to estimate the fluid forces on the bars. For a 2D problem, each segment (including the head) has three degrees of freedom, and the trajectory of the micro-swimmer can be manifested by the time history of the location of the head centroid. The balance of momentum of each segment, as well as the head,

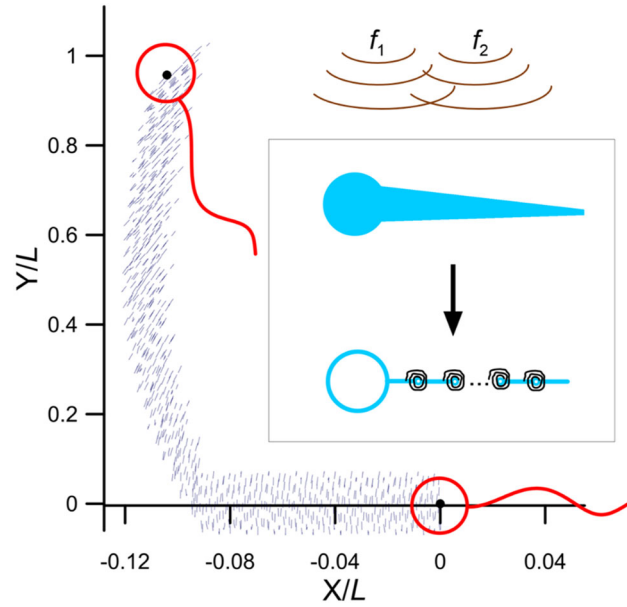


Fig. 8. Turning mechanism based on two-frequency acoustic waves. L is the length of the tail, which is $180\ \mu\text{m}$

will lead to the governing equations in the form of ODEs, which can be solved numerically. Since the external excitations will eventually appear in the boundary conditions at the head, it is straightforward to adjust the governing equations according to external excitations.

The turning mechanism demonstrated in Fig. 8 involves two piezoelectric acoustic transducers (commercially available) with frequencies $f_1 = 3.6\ \text{kHz}$ and $f_2 = 4.6\ \text{kHz}$ [171]. In this strategy, what matters is breaking the harmonicity of the symmetrically lateral motion. A special on-off function is added to the f_2 acoustic transducer to break the harmonicity in each of the common periods of the two-frequency acoustic waves. When the on-off function is inactive, the trajectory is horizontal. The swimmer will start to align with the Y -axis when the special on-off function of the f_2 acoustic transducer is turned on. It has also been noted that the swimmer oscillates symmetrically about the X -axis (the mean trajectory is still straight) if the on-off function is not applied. The role of the on-off function is to break the symmetry at a series of “right” moments to prompt the direction change; therefore, these “right” moments must be different from the common periods of f_1 and f_2 . However, this steering strategy could be difficult to implement because the sharp on-off function is practically unachievable. Therefore, the steering strategy shown in Fig. 9 seems more feasible, where the acoustic waves are exploited to propel the swimmer, and a magnetic-induced torque is exerted to the head to turn the swimmer. This magnetic torque can be implemented via embedding magnetic nanoparticles into the head. As exhibited in Fig. 9a, the magnetic torque was on only for a certain time. When the magnetic torque vanished (at around Period 500 as shown in Fig. 9a), the acoustic wave changed its direction by 90° to continue propelling the swimmer along the new orientation. The value of magnetization \mathbf{m} of the magnetic nanoparticles used in hyperthermia-based therapy is usually between 8 and 16 kA/m [234], and the corresponding magnetic flux density will be around $4 \times 10^{-15}\ \text{T}$, which is sufficiently safe for most applications. Note that the degree of the wavevector is about the X -axis shown in Fig. 9b, and compared with Fig. 9a, b, one may find that the principal advance direction of the micro-swimmer is perpendicular to the acoustic wavevector.

5. Outlook

In this article, it has been aimed to elucidate the theoretical framework which is essential to fathom the dynamic behaviors of natural and artificial swimmers at LRNs. We first reviewed the studies on microorganisms, which are reminiscent of the propulsive mechanisms of natural micro-swimmers. After reviewing the basic principles and the development of the understanding of them, we took the flagellated

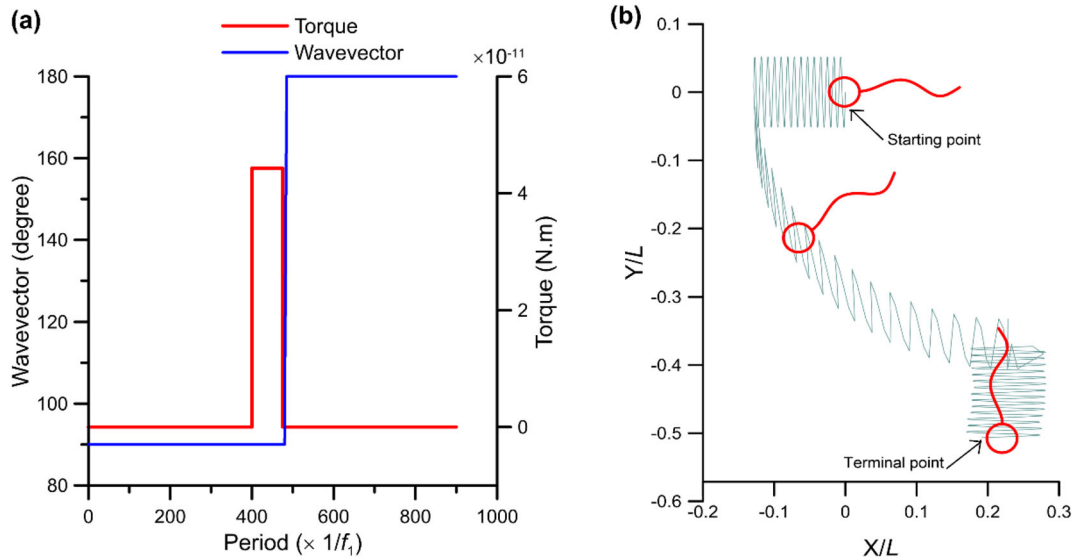


Fig. 9. The effect of the head magnetic torque on the micro-swimmer turning: **a** the amplitude of the magnetic torque and the direction of the acoustic wavevector, with f_1 the actuation frequency, which is 3600 Hz; **b** the trajectory of the head centroid and the configurations of the swimmer at three instants, with $L = 180\mu\text{m}$ the length of the tail

micro-swimmers as an example to elaborate on the theories of their locomotion. We then reviewed the progress in actuation strategies, such as the magnetic and acoustic actuations, of artificial flagellated micro-swimmers, and finally proposed two possible strategies to realize the turning of a flagellated micro-swimmer—the key step toward manipulation through remote fields. Despite these impressive advances made in the field, inadequacies need to be addressed particularly when the applications require high accuracy and controllability.

First, the present experimental validation for theoretical models, such as the RFT and SBT, is inadequate due to the difficulties caused by the small scale. Hence, in view of the advancement of the experimental techniques, prospective work for further revealing the mechanisms of these micro-swimmers with more comprehensive experimental validation is of great significance and worth exploring. Second, the practical world is complex and Reynolds numbers are nonzero; therefore, simple theories based on the Stokes equations are insufficient. Numerical simulations are in principle the most powerful theoretical tool with the development of computational power. Thus, more studies dealing with multi-physical couplings, e.g., the entanglement of fluids, acoustic waves, and flexible swimmers, are imminently essential. There is certainly much room for improving the performance of numerical simulations. The auto-remeshing technique has been reported, which may be a breakthrough for solving fluid–structure interactions coupled with rigid body motion. The geometry optimization based on numerical simulations of an artificial micro-swimmer is more valuable for application, which should be the next research focus. Finally, although some *in vivo* experiments with externally powered artificial micro-swimmers have been attempted, there exists a huge gap between laboratory studies and practical applications. The study of the strategies for precise and robust manipulation of artificial micro-swimmers is still in its infancy, which should be the pivotal factor for enabling their applications. Our studies in Sect. 4 theoretically realized the steering of a flagellated micro-swimmer under external actuation. Further investigations could focus on the trajectory planning for demanded application. For example, how to make the swimmer stagnate to implement some targeted missions (e.g., drug release or thermotherapy), how to precisely control its trajectory to pass through a complex biological duct, *etc.* The strategy we proposed, which is to propel by acoustic waves and turn by a magnetic field, may be a feasible scheme to realize steering. The next studies should focus on the experimental implementation of swimmer navigation. The control system of the magnetic field should be designed, and the fabrication technique of micro-swimmer with magnetic nanoparticles must also be explored. The visualization and precious steering of swimmers *in vivo* may be the further consideration

when it comes to a medical application. It is not straightforward to overcome these interdisciplinary challenges. Scientists in various fields should cooperate to achieve the leap from laboratory trials to practical applications.

Acknowledgements. The first author is supported by the General Research Fund of Hong Kong RGC (Grant No. 15213619). The second author is supported by the postdoctoral scheme of the Hong Kong Polytechnic University (Project ID: P0034926). The studies presented in this work are supported by the NSFC/RGC Joint Research Scheme (RGC: *N_PolyU519/19* and NSFC: 51961160729). The authors are grateful for these financial supports.

Author contributions The manuscript was written based on the contributions made by all authors (JL, YF, XL and HR): XL and HR devised the project, the main conceptual ideas, and proof outline. JL worked out almost all of the technical details and performed most of the writing. YF and HR were involved in all discussions and performed the writing. HR is the corresponding author.

Declarations

Conflict of interest The authors declare that they have no known competing financial interests or personal relationships that could have appeared to influence the work reported in this paper.

Availability of Data and Materials The authors confirm that the data required to reproduce the findings of this study are available within the article and can be reproduced.

Code Availability All codes are available upon request.

Consent for Publication This article has been approved by all the authors for publication.

References

- [1] Feynman RP. There's plenty of room at the bottom [data storage]. *J Microelectromech Syst.* 1992;1(1):60–6.
- [2] Esteban-Fernández de Ávila B, et al. Micromotors go in vivo: from test tubes to live animals. *Adv Funct Mater.* 2018;28(25):1705640.
- [3] Halder A, Sun Y. Biocompatible propulsion for biomedical micro/nano robotics. *Biosens Bioelectron.* 2019;139:111334.
- [4] Fischer P, Nelson BJ, Yang G-Z. New materials for next-generation robots. *Sci Robot.* 2018;3(18):eaau0448.
- [5] Patra D, et al. Intelligent, self-powered, drug delivery systems. *Nanoscale.* 2013;5(4):1273–83.
- [6] Ma X, Hahn K, Sanchez S. Catalytic mesoporous Janus nanomotors for active cargo delivery. *J Am Chem Soc.* 2015;137(15):4976–9.
- [7] Medina-Sánchez M, et al. Cellular cargo delivery: toward assisted fertilization by sperm-carrying micromotors. *Nano Lett.* 2016;16(1):555–61.
- [8] Walker D, et al. Enzymatically active biomimetic micropropellers for the penetration of mucin gels. *Sci Adv.* 2015;1(11):e1500501.
- [9] Miyashita S, et al. Ingestible, controllable, and degradable origami robot for patching stomach wounds. In: 2016 IEEE international conference on robotics and automation (ICRA). 2016. IEEE.
- [10] Soler L, et al. Self-propelled micromotors for cleaning polluted water. *ACS Nano.* 2013;7(11):9611–20.
- [11] Soler L, Sánchez S. Catalytic nanomotors for environmental monitoring and water remediation. *Nanoscale.* 2014;6(13):7175–82.
- [12] Vilela D, et al. Graphene-based microbots for toxic heavy metal removal and recovery from water. *Nano Lett.* 2016;16(4):2860–6.
- [13] Mallouk TE, Sen A. Nanotechnology-Powering Nanorobots-Catalytic engines enable tiny swimmers to harness fuel from their environment and overcome the weird physics of the microscopic world. *Sci Am.* 2009;300(5):72–77.
- [14] Lighthill J. Flagellar hydrodynamics. *SIAM Rev.* 1976;18(2):161–230.
- [15] Lighthill J. Helical distributions of Stokeslets. *J Eng Math.* 1996;30(1–2):35–78.
- [16] Lauga E, Powers TR. The hydrodynamics of swimming microorganisms. *Rep Prog Phys.* 2009;72(9):096601.
- [17] Pak OS, et al. Theoretical models of low-Reynolds-number locomotion. In: Fluid–structure interactions in low-Reynolds-number flows. Royal Society of Chemistry; 2015. p. 100–67.

- [18] Lauga E. Bacterial hydrodynamics. *Annu Rev Fluid Mech.* 2016;48:105–30.
- [19] Elgeti J, Winkler RG, Gompper G. Physics of microswimmers-single particle motion and collective behavior: a review. *Rep Prog Phys.* 2015;78(5):056601.
- [20] Bechinger C, et al. Active particles in complex and crowded environments. *Rev Mod Phys.* 2016;88(4):045006.
- [21] Zhang L, et al. Artificial bacterial flagella: Fabrication and magnetic control. *Appl Phys Lett.* 2009;94(6):064107.
- [22] Sánchez S, Soler L, Katuri J. Chemically powered micro-and nanomotors. *Angew Chem Int Ed.* 2015;54(5):1414–44.
- [23] Rao KJ, et al. A force to be reckoned with: a review of synthetic microswimmers powered by ultrasound. *Small.* 2015;11(24):2836–46.
- [24] Mohanty S, Khalil IS, Misra S. Contactless acoustic micro/nano manipulation: a paradigm for next generation applications in life sciences. *Proc R Soc A.* 2020;476(2243):20200621.
- [25] Sitti M, et al. Biomedical applications of untethered mobile milli/microrobots. *Proc IEEE.* 2015;103(2):205–24.
- [26] Zhou H, et al. Magnetically driven micro and nanorobots. *Chem Rev.* 2021;121(8):4999–5041.
- [27] Eshaghi M, Ghasemi M, Khorshidi K. Design, manufacturing and applications of small-scale magnetic soft robots. *Extreme Mech Lett.* 2021;44:101268. <https://doi.org/10.1016/j.eml.2021.101268>.
- [28] Wang L, et al. Engineering magnetic micro/nanorobots for versatile biomedical applications. *Adv Intell Syst.* 2021;3(7):2000267. <https://doi.org/10.1002/aisy.202000267>.
- [29] Cho SK. Mini and micro propulsion for medical swimmers. *Micromachines.* 2014;5(1):97–113.
- [30] Chen XZ, et al. Small-scale machines driven by external power sources. *Adv Mater.* 2018;30(15):1705061.
- [31] Baker R, Brooks AM, Sen A. Designing Proteus: engineering form and function for microrobotics. In: *Robotic systems and autonomous platforms.* Elsevier; 2019. p. 85–108.
- [32] Soto F, et al. Medical micro/nanorobots in precision medicine. *Adv Sci.* 2020;7(21):2002203.
- [33] Abbott JJ, Peyer KE, Lagomarsino MC, Zhang L, Dong L, Kaliakatsos IK, Nelson BJ. How should microrobots swim? *Int J Robot Res.* 2009;28(11–12):1434–47.
- [34] Dobell C (Ed.). *A Collection of Writings by the Father of Protozoology and Bacteriology, Antony Van Leeuwenhoek and His “Little Animals”.* Dover Publications; 1960.
- [35] Berg H. Motile behavior of bacteria. *Phys Today.* 2000.
- [36] Berg HC. The rotary motor of bacterial flagella. *Annu Rev Biochem.* 2003;72.
- [37] Berg H. *E. coli in motion.* New York: Springer; 2004.
- [38] Turner L, Ryu WS, Berg HC. Real-time imaging of fluorescent flagellar filaments. *J Bacteriol.* 2000;182(10):2793–801.
- [39] Lowe G, Meister M, Berg HC. Rapid rotation of flagellar bundles in swimming bacteria. *Nature.* 1987;325(6105):637–40.
- [40] Bray D. *Cell movements: from molecules to motility.* ISBN 9780815332824. Published November 23, 2000 by Garland Science.
- [41] Koyasu S, Shirakihara Y. *Caulobacter crescentus* flagellar filament has a right-handed helical form. *J Mol Biol.* 1984;173(1):125–30.
- [42] Armitage JP, Schmitt R. Bacterial chemotaxis: *Rhodobacter sphaeroide* and *Sinorhizobium meliloti*-variations on a theme? *Microbiology.* 1997;143(12):3671–82.
- [43] Krieg NR, Manual H. *Systematic bacteriology.* Baltimore: Williams; 1984.
- [44] Buller AHR. Is chemotaxis a factor in the fertilisation of the eggs of animals? *Q J Microscop Sci.* 1903;46:145–76.
- [45] Rothschild L, Swann M. The fertilization reaction in the sea-urchin: the probability of a successful sperm-egg collision. *J Exp Biol.* 1951;28(3):403–16.
- [46] Gray J. The movement of sea-urchin spermatozoa. *J Exp Biol.* 1955;32(4):775–801.
- [47] Rikmenspoel R, Van Herpen G, Eijkhout P. Cinematographic observations of the movements of bull sperm cells. *Phys Med Biol.* 1960;5(2):167.
- [48] Rothschild L, Swann M. The fertilization reaction in the sea-urchin egg. The effect of nicotine. *J Exp Biol.* 1950;27(3):400–6.
- [49] Brokaw C. Non-sinusoidal bending waves of sperm flagella. *J Exp Biol.* 1965;43(1):155–69.
- [50] Brokaw CJ. Bending moments in free-swimming flagella. *J Exp Biol.* 1970;53(2):445–64.
- [51] Stearns J, Surette M. *Microbiology for dummies.* New York: Wiley; 2019.
- [52] Childress S. *Mechanics of swimming and flying.* Cambridge: Cambridge University Press; 1981.
- [53] Brennen C, Winet H. Fluid mechanics of propulsion by cilia and flagella. *Annu Rev Fluid Mech.* 1977;9(1):339–98.

- [54] Ellington CP. The aerodynamics of hovering insect flight. II. Morphological parameters. *Philos Trans R Soc Lond B Biol Sci.* 1984;305(1122):17–40.
- [55] Vogel E, Vogel D. *Kindred strangers: the uneasy relationship between politics and business in America*, vol. 155. Princeton: Princeton University Press; 1996.
- [56] Alexander DE. *Nature's flyers: birds, insects, and the biomechanics of flight*. Baltimore: JHU Press; 2002.
- [57] Dudley R. *The biomechanics of insect flight: form, function, evolution*. Princeton: Princeton University Press; 2002.
- [58] Vogel S. *Comparative biomechanics: life's physical world*. Princeton: Princeton University Press; 2003.
- [59] Ludwig W. Zur theorie der flimmerbewegung (dynamik, nutzeffekt, energiebilanz). *Z Vgl Physiol.* 1930;13(3):397–504.
- [60] Lighthill J. *Mathematical biofluidynamics*. Philadelphia: SIAM; 1975.
- [61] Lighthill SJ. Flagellar hydrodynamics: the von Neumann Lecture, 1975. *SIAM Rev.* 1976;18(2):161–230.
- [62] Purcell EM. Life at low Reynolds number. *Am J Phys.* 1977;45(1):3–11.
- [63] Yates GT. How microorganisms move through water: the hydrodynamics of ciliary and flagellar propulsion reveal how microorganisms overcome the extreme effect of the viscosity of water. *Am Sci.* 1986;74(4):358–65.
- [64] Taylor G, Triantafyllou MS, Tropea C. *Animal locomotion*. Berlin: Springer; 2010.
- [65] Holwill MEJ. Physical aspects of Flagellar movement. *Physiol Rev.* 1966;46(4):696–785.
- [66] Hinch E. Hydrodynamics at low Reynolds numbers: a brief and elementary introduction. In: *Disorder and mixing*. Springer, Berlin;1988. p. 43–56.
- [67] Lighthill SJ. *Mathematical biofluidynamics*. Philadelphia: SIAM; 1975.
- [68] Gray J, Hancock G. The propulsion of sea-urchin spermatozoa. *J Exp Biol.* 1955;32(4):802–14.
- [69] Becker LE, Koehler SA, Stone HA. On self-propulsion of micro-machines at low Reynolds number: Purcell's three-link swimmer. *J Fluid Mech.* 2003;490:15.
- [70] Childress S, Dudley R. Transition from ciliary to flapping mode in a swimming mollusc: flapping flight as a bifurcation in Re . *J Fluid Mech.* 2004;498:257–88.
- [71] Alben S, Shelley M. Coherent locomotion as an attracting state for a free flapping body. *Proc Natl Acad Sci.* 2005;102(32):11163–6.
- [72] Vandenberghe N, Childress S, Zhang J. On unidirectional flight of a free flapping wing. *Phys Fluids.* 2006;18(1):014102.
- [73] Lu X-Y, Liao Q. Dynamic responses of a two-dimensional flapping foil motion. *Phys Fluids.* 2006;18(9):098104.
- [74] Lauga E. Continuous breakdown of Purcell's scallop theorem with inertia. *Phys Fluids.* 2007;19(6):061703.
- [75] Friedrich BM, et al. High-precision tracking of sperm swimming fine structure provides strong test of resistive force theory. *J Exp Biol.* 2010;213(8):1226–34.
- [76] Sznitman J, et al. Propulsive force measurements and flow behavior of undulatory swimmers at low Reynolds number. *Phys Fluids.* 2010;22(12):121901.
- [77] Bayly P, et al. Propulsive forces on the flagellum during locomotion of *Chlamydomonas reinhardtii*. *Biophys J.* 2011;100(11):2716–25.
- [78] Maladen RD, et al. Mechanical models of sandfish locomotion reveal principles of high performance subsurface sand-swimming. *J R Soc Interface.* 2011;8(62):1332–45.
- [79] Lauga E, et al. Swimming in circles: motion of bacteria near solid boundaries. *Biophys J.* 2006;90(2):400–12.
- [80] Chattopadhyay S, et al. Swimming efficiency of bacterium *Escherichia coli*. *Proc Natl Acad Sci.* 2006;103(37):13712–7.
- [81] Chattopadhyay S, Wu X-L. The effect of long-range hydrodynamic interaction on the swimming of a single bacterium. *Biophys J.* 2009;96(5):2023–8.
- [82] Darnton NC, et al. On torque and tumbling in swimming *Escherichia coli*. *J Bacteriol.* 2007;189(5):1756–64.
- [83] Vogel R, Stark H. Force-extension curves of bacterial flagella. *Eur Phys J E.* 2010;33(3):259–71.
- [84] Vogel R, Stark H. Motor-driven bacterial flagella and buckling instabilities. *Eur Phys J E.* 2012;35(2):1–15.
- [85] Behkam BM. Design methodology for biomimetic propulsion of miniature swimming robots. *Sitti*;2006.
- [86] Li H, Tan J, Zhang M. Dynamics modeling and analysis of a swimming microrobot for controlled drug delivery. *IEEE Trans Autom Sci Eng.* 2008;6(2):220–7.
- [87] NgocSan H, NamSeo G, HyeonKyu Y. Development of a propulsion system for a biomimetic thruster. *Chin Sci Bull.* 2011;56:432–8.

- [88] Rorai C, Zaitsev M, Karabasov S. On the limitations of some popular numerical models of flagellated microswimmers: importance of long-range forces and flagellum waveform. *R Soc Open Sci.* 2019;6(1):180745.
- [89] Johnson RE. An improved slender-body theory for Stokes flow. *J Fluid Mech.* 1980;99(2):411–31.
- [90] Cortez R, Fauci L, Medovikov A. The method of regularized Stokeslets in three dimensions: analysis, validation, and application to helical swimming. *Phys Fluids.* 2005;17(3):031504.
- [91] Hancock G. The self-propulsion of microscopic organisms through liquids. *Proc R Soc Lond Ser A Math Phys Sci.* 1953;217(1128):96–121.
- [92] Garcia-Gonzalez J. Numerical analysis of fluid motion at low Reynolds numbers. Manchester: The University of Manchester; 2017.
- [93] Tabak AF, Yesilyurt S. Computationally-validated surrogate models for optimal geometric design of bio-inspired swimming robots: Helical swimmers. *Comput Fluids.* 2014;99:190–8.
- [94] Rodenborn B, et al. Propulsion of microorganisms by a helical flagellum. *Proc Natl Acad Sci.* 2013;110(5):E338–47.
- [95] Ramia M, Tullock D, Phan-Thien N. The role of hydrodynamic interaction in the locomotion of microorganisms. *Biophys J.* 1993;65(2):755–78.
- [96] Shum H, Gaffney E, Smith D. Modelling bacterial behaviour close to a no-slip plane boundary: the influence of bacterial geometry. *Proc R Soc A Math Phys Eng Sci.* 2010;466(2118):1725–48.
- [97] Pimponi D, et al. Hydrodynamics of flagellated microswimmers near free-slip interfaces. *J Fluid Mech.* 2016;789:514–33.
- [98] Pimponi D, Chinappi M, Gualtieri P. Flagellated microswimmers: hydrodynamics in thin liquid films. *European Phys J E.* 2018;41(2):1–8.
- [99] Curatolo M, Teresi L. Modeling and simulation of fish swimming with active muscles. *J Theor Biol.* 2016;409:18–26.
- [100] Taylor GI. Analysis of the swimming of microscopic organisms. *Proc R Soc Lond Ser A Math Phys Sci.* 1951;209(1099):447–61.
- [101] Chwang A, Wu TY. A note on the helical movement of micro-organisms. *Proc R Soc Lond Ser B Biol Sci.* 1971;178(1052):327–46.
- [102] Lighthill M. On the squirming motion of nearly spherical deformable bodies through liquids at very small Reynolds numbers. *Commun Pure Appl Math.* 1952;5(2):109–18.
- [103] Blake JR. A spherical envelope approach to ciliary propulsion. *J Fluid Mech.* 1971;46(1):199–208.
- [104] Blake J. Self propulsion due to oscillations on the surface of a cylinder at low Reynolds number. *Bull Austral Math Soc.* 1971;5(2):255–64.
- [105] Reynolds A. The swimming of minute organisms. *J Fluid Mech.* 1965;23(2):241–60.
- [106] Tuck E. A note on a swimming problem. *J Fluid Mech.* 1968;31(2):305–8.
- [107] Machin K. Wave propagation along flagella. *J Exp Biol.* 1958;35(4):796–806.
- [108] Machin K. The control and synchronization of Flagellar movement. *Proc R Soc Lond Ser B Biol Sci.* 1963;158(970):88–104.
- [109] Wiggins CH, Goldstein RE. Flexive and propulsive dynamics of elastica at low Reynolds number. *Phys Rev Lett.* 1998;80(17):3879.
- [110] Lowe CP. Dynamics of filaments: modelling the dynamics of driven microfilaments. *Philos Trans R Soc Lond Ser B Biol Sci.* 2003;358(1437):1543–50.
- [111] Lagomarsino MC, Capuani F, Lowe CP. A simulation study of the dynamics of a driven filament in an Aristotelian fluid. *J Theor Biol.* 2003;224(2):215–24.
- [112] Yu TS, Lauga E, Hosoi A. Experimental investigations of elastic tail propulsion at low Reynolds number. *Phys Fluids.* 2006;18(9):091701.
- [113] Lauga E. Floppy swimming: viscous locomotion of actuated elastica. *Phys Rev E.* 2007;75(4):041916.
- [114] Kosa G, Shoham M, Zaaroor M. Propulsion method for swimming microrobots. *IEEE Trans Robot.* 2007;23(1):137–50.
- [115] Fu HC, Wolgemuth CW, Powers TR. Beating patterns of filaments in viscoelastic fluids. *Phys Rev E.* 2008;78(4):041913.
- [116] Riveline D, et al. Elastohydrodynamic study of actin filaments using fluorescence microscopy. *Phys Rev E.* 1997;56(2):R1330.
- [117] Wiggins CH, et al. Trapping and wiggling: elastohydrodynamics of driven microfilaments. *Biophys J.* 1998;74(2):1043–60.
- [118] Dreyfus R, et al. Microscopic artificial swimmers. *Nature.* 2005;437(7060):862–5.
- [119] Liu J, Ruan H. Modeling of an acoustically actuated artificial micro-swimmer. *Bioinspir Biomim.* 2020;15(3):036002.

- [120] Singh TS, Yadava R. Effect of tapering on elastic filament microswimming under planar body actuation. *Biomed Phys Eng Express*. 2017;4(1):015019.
- [121] Manikantan H, Saintillan D. Buckling transition of a semiflexible filament in extensional flow. *Phys Rev E*. 2015;92(4):041002.
- [122] Kantsler V, Goldstein RE. Fluctuations, dynamics, and the stretch-coil transition of single actin filaments in extensional flows. *Phys Rev Lett*. 2012;108(3):038103.
- [123] Guglielmini L, et al. Buckling transitions of an elastic filament in a viscous stagnation point flow. *Phys Fluids*. 2012;24(12):123601.
- [124] Manikantan H, Saintillan D. Subdiffusive transport of fluctuating elastic filaments in cellular flows. *Phys Fluids*. 2013;25(7):073603.
- [125] Young Y-N, Shelley MJ. Stretch-coil transition and transport of fibers in cellular flows. *Phys Rev Lett*. 2007;99(5):058303.
- [126] Wandersman E, et al. Buckled in translation. *Soft Matter*. 2010;6(22):5715–9.
- [127] Hinch E. The distortion of a flexible inextensible thread in a shearing flow. *J Fluid Mech*. 1976;74(2):317–33.
- [128] Becker LE, Shelley MJ. Instability of elastic filaments in shear flow yields first-normal-stress differences. *Phys Rev Lett*. 2001;87(19):198301.
- [129] Tornberg A-K, Shelley MJ. Simulating the dynamics and interactions of flexible fibers in Stokes flows. *J Comput Phys*. 2004;196(1):8–40.
- [130] Munk T, et al. Dynamics of semiflexible polymers in a flow field. *Phys Rev E*. 2006;74(4):041911.
- [131] Young Y-N. Hydrodynamic interactions between two semiflexible inextensible filaments in Stokes flow. *Phys Rev E*. 2009;79(4):046317.
- [132] Harasim M, et al. Direct observation of the dynamics of semiflexible polymers in shear flow. *Phys Rev Lett*. 2013;110(10):108302.
- [133] Steinhauser D, Köster S, Pfohl T. Mobility gradient induces cross-streamline migration of semiflexible polymers. *ACS Macro Lett*. 2012;1(5):541–5.
- [134] Autrusson N, et al. The shape of an elastic filament in a two-dimensional corner flow. *Phys Fluids*. 2011;23(6):063602.
- [135] Wexler JS, et al. Bending of elastic fibres in viscous flows: the influence of confinement. *J Fluid Mech*. 2013;720:517–44.
- [136] Seifert U, Wintz W, Nelson P. Straightening of thermal fluctuations in semiflexible polymers by applied tension. *Phys Rev Lett*. 1996;77(27):5389.
- [137] Llopis I, et al. Sedimentation of pairs of hydrodynamically interacting semiflexible filaments. *Phys Rev E*. 2007;76(6):061901.
- [138] Spagnolie SE, Lauga E. The optimal elastic flagellum. *Phys Fluids*. 2010;22(3):455.
- [139] Jayaraman G, et al. Autonomous motility of active filaments due to spontaneous flow-symmetry breaking. *Phys Rev Lett*. 2012;109(15):158302.
- [140] Evans AA, et al. Elastocapillary self-folding: buckling, wrinkling, and collapse of floating filaments. *Soft Matter*. 2013;9(5):1711–20.
- [141] Parmar J, et al. Nano and micro architectures for self-propelled motors. *Sci Technol Adv Mater*. 2015;16(1):014802.
- [142] Wang H, Pumera M. Fabrication of micro/nanoscale motors. *Chem Rev*. 2015;115(16):8704–35.
- [143] Wang W, et al. From one to many: dynamic assembly and collective behavior of self-propelled colloidal motors. *Accounts Chem Res*. 2015;48(7):1938–46.
- [144] Katuri J, et al. Designing micro-and nanoswimmers for specific applications. *Accounts Chem Res*. 2017;50(1):2–11.
- [145] Maric T, et al. Black-phosphorus-enhanced bubble-propelled autonomous catalytic microjets. *Appl Mater Today*. 2017;9:289–91.
- [146] Paxton WF, et al. Catalytic nanomotors: autonomous movement of striped nanorods. *J Am Chem Soc*. 2004;126(41):13424–31.
- [147] Fournier-Bidoz S, et al. Synthetic self-propelled nanomotors. *Chem Commun*. 2005;4:441–3.
- [148] Paxton WF, Sen A, Mallouk TE. Motility of catalytic nanoparticles through self-generated forces. *Chem-A Eur J*. 2005;11(22):6462–70.
- [149] Sundararajan S, et al. Catalytic motors for transport of colloidal cargo. *Nano Lett*. 2008;8(5):1271–6.
- [150] Sundararajan S, et al. Drop-off of colloidal cargo transported by catalytic Pt–Au nanomotors via photochemical stimuli. *Small*. 2010;6(14):1479–82.
- [151] Kagan D, et al. Rapid delivery of drug carriers propelled and navigated by catalytic nanoshuttles. *Small*. 2010;6(23):2741–7.

- [152] Xu T, Xu L-P, Zhang X. Ultrasound propulsion of micro-/nanomotors. *Appl Mater Today*. 2017;9:493–503.
- [153] Chen X-Z, et al. Recent developments in magnetically driven micro-and nanorobots. *Appl Mater Today*. 2017;9:37–48.
- [154] Bell DJ, et al. Flagella-like propulsion for microrobots using a nanocoil and a rotating electromagnetic field. In: *Proceedings 2007 IEEE international conference on robotics and automation*. 2007. IEEE.
- [155] Hawkeye MM, Brett MJ. Glancing angle deposition: fabrication, properties, and applications of micro-and nanostructured thin films. *J Vac Sci Technol A Vac Surf Films*. 2007;25(5):1317–35.
- [156] Schuerle S, et al. Helical and tubular lipid microstructures that are electroless-coated with CoNiReP for wireless magnetic manipulation. *Small*. 2012;8(10):1498–502.
- [157] Gao W, et al. Bioinspired helical microswimmers based on vascular plants. *Nano Lett*. 2014;14(1):305–10.
- [158] Fusco S, et al. An integrated microrobotic platform for on-demand, targeted therapeutic interventions. *Adv Mater*. 2014;26(6):952–7.
- [159] Fusco S, et al. Shape-switching microrobots for medical applications: the influence of shape in drug delivery and locomotion. *ACS Appl Mater Interfaces*. 2015;7(12):6803–11.
- [160] Huang H-W, et al. Soft micromachines with programmable motility and morphology. *Nat Commun*. 2016;7(1):1–10.
- [161] Khalil IS, et al. MagnetoSperm: a microrobot that navigates using weak magnetic fields. *Appl Phys Lett*. 2014;104(22):223701.
- [162] Li T, et al. Magnetically propelled fish-like nanoswimmers. *Small*. 2016;12(44):6098–105.
- [163] Wang W, et al. Autonomous motion of metallic microrods propelled by ultrasound. *ACS Nano*. 2012;6(7):6122–32.
- [164] Ahmed S, et al. Self-assembly of nanorod motors into geometrically regular multimers and their propulsion by ultrasound. *ACS Nano*. 2014;8(11):11053–60.
- [165] Ahmed S, et al. Steering acoustically propelled nanowire motors toward cells in a biologically compatible environment using magnetic fields. *Langmuir*. 2013;29(52):16113–8.
- [166] Garcia-Gradilla V, et al. Functionalized ultrasound-propelled magnetically guided nanomotors: toward practical biomedical applications. *ACS Nano*. 2013;7(10):9232–40.
- [167] Ahmed D, et al. Selectively manipulable acoustic-powered microswimmers. *Sci Rep*. 2015;5(1):1–8.
- [168] Feng J, Yuan J, Cho SK. Micropropulsion by an acoustic bubble for navigating microfluidic spaces. *Lab on a Chip*. 2015;15(6):1554–62.
- [169] Ahmed D, et al. Artificial acousto-magnetic soft microswimmers. *Adv Mater Technol*. 2017;2(7):1700050.
- [170] Ahmed D, et al. Artificial swimmers propelled by acoustically activated flagella. *Nano Lett*. 2016;16(8):4968–74.
- [171] Kaynak M, et al. Acoustic actuation of bioinspired microswimmers. *Lab on a Chip*. 2017;17(3):395–400.
- [172] Jiang H-R, Yoshinaga N, Sano M. Active motion of a Janus particle by self-thermophoresis in a defocused laser beam. *Phys Rev Lett*. 2010;105(26):268302.
- [173] Ni M, et al. A review and recent developments in photocatalytic water-splitting using TiO₂ for hydrogen production. *Renew Sustain Energy Rev*. 2007;11(3):401–25.
- [174] Ibele M, Mallouk TE, Sen A. Schooling behavior of light-powered autonomous micromotors in water. *Angew Chem*. 2009;121(18):3358–62.
- [175] Duan W, et al. Motion analysis of light-powered autonomous silver chloride nanomotors. *Eur Phys J E*. 2012;35(8):1–8.
- [176] Erdem EY, et al. Thermally actuated omnidirectional walking microrobot. *J Microelectromech Syst*. 2010;19(3):433–42.
- [177] Saito K, et al. Miniaturized rotary actuators using shape memory alloy for insect-type MEMS microrobot. *Micromachines*. 2016;7(4):58.
- [178] Saito K, et al. Insect-type MEMS microrobot with mountable bare chip IC of artificial neural networks. *Artif Life Robot*. 2017;22(1):118–24.
- [179] Darhuber AA, et al. Microfluidic actuation by modulation of surface stresses. *Appl Phys Lett*. 2003;82(4):657–9.
- [180] Jiao Z, Huang X, Nguyen N-T. Manipulation of a droplet in a planar channel by periodic thermocapillary actuation. *J Micromech Microeng*. 2008;18(4):045027.
- [181] Hosseinidoust Z, et al. Bioengineered and biohybrid bacteria-based systems for drug delivery. *Adv Drug Deliv Rev*. 2016;106:27–44.
- [182] Schwarz L, Medina-Sánchez M, Schmidt OG. Hybrid biomicromotors. *Appl Phys Rev*. 2017;4(3):031301.
- [183] Lu AX, et al. Catalytic propulsion and magnetic steering of soft, patchy microcapsules: ability to pick-up and drop-off microscale cargo. *ACS Appl Mater Interfaces*. 2016;8(24):15676–83.

- [184] Singh AK, et al. Multimodal chemo-magnetic control of self-propelling microbots. *Nanoscale*. 2014;6(3):1398–405.
- [185] Jang B, et al. Undulatory locomotion of magnetic multilink nanoswimmers. *Nano Lett*. 2015;15(7):4829–33.
- [186] Bertin N, et al. Propulsion of bubble-based acoustic microswimmers. *Phys Rev Appl*. 2015;4(6):064012.
- [187] Peyer KE, Zhang L, Nelson BJ. Localized non-contact manipulation using artificial bacterial flagella. *Appl Phys Lett*. 2011;99(17):174101.
- [188] Peyer KE, Zhang L, Nelson BJ. Bio-inspired magnetic swimming microrobots for biomedical applications. *Nanoscale*. 2013;5(4):1259–72.
- [189] Nama N, et al. Investigation of acoustic streaming patterns around oscillating sharp edges. *Lab on a Chip*. 2014;14(15):2824–36.
- [190] Dijkink R, et al. The ‘acoustic scallop’: a bubble-powered actuator. *J Micromech Microeng*. 2006;16(8):1653.
- [191] Oguz H, Prosperetti A. The natural frequency of oscillation of gas bubbles in tubes. *J Acoust Soc Am*. 1998;103(6):3301–8.
- [192] Ren L, et al. 3D steerable, acoustically powered microswimmers for single-particle manipulation. *Sci Adv*. 2019;5(10):eaax3084.
- [193] Finnie I, Curl RL. Physics in a toy boat. *Am J Phys*. 1963;31(4):289–93.
- [194] Yang T-Z, et al. Microfluid-induced nonlinear free vibration of microtubes. *Int J Eng Sci*. 2014;76:47–55.
- [195] Lei Y, Adhikari S, Friswell M. Vibration of nonlocal Kelvin–Voigt viscoelastic damped Timoshenko beams. *Int J Eng Sci*. 2013;66:1–13.
- [196] Ghayesh MH. Viscoelastic dynamics of axially FG microbeams. *Int J Eng Sci*. 2019;135:75–85.
- [197] Ghayesh MH, Farokhi H, Hussain S. Viscoelastically coupled size-dependent dynamics of microbeams. *Int J Eng Sci*. 2016;109:243–55.
- [198] Brokaw CJ. Bend propagation by a sliding filament model for flagella. *J Exp Biol*. 1971;55(2):289–304.
- [199] Ming T, Ding Y. Transition and formation of the torque pattern of undulatory locomotion in resistive force dominated media. *Bioinspir Biomimet*. 2018;13(4):046001.
- [200] Berg HC, Anderson RA. Bacteria swim by rotating their flagellar filaments. *Nature*. 1973;245(5425):380–2.
- [201] Thomas D, Morgan DG, DeRosier DJ. Structures of bacterial flagellar motors from two FliF–FliG gene fusion mutants. *J Bacteriol*. 2001;183(21):6404.
- [202] Darnton NC, et al. On torque and tumbling in swimming *Escherichia coli*. *J Bacteriol*. 2007;189(5):1756.
- [203] Jawed MK, et al. Propulsion and instability of a flexible helical rod rotating in a viscous fluid. *Phys Rev Lett*. 2015;115(16):168101.
- [204] Zöttl A, Yeomans JM. Enhanced bacterial swimming speeds in macromolecular polymer solutions. *Nat Phys*. 2019;15(6):554–8.
- [205] Angeles V, et al. Front-back asymmetry controls the impact of viscoelasticity on helical swimming. *Phys Rev Fluids*. 2021;6(4):043102.
- [206] Zhang J, Chinappi M, Biferale L. Base flow decomposition for complex moving objects in linear hydrodynamics: application to helix-shaped flagellated microswimmers. *Phys Rev E*. 2021;103(2):023109.
- [207] Ghosh A, Fischer P. Controlled propulsion of artificial magnetic nanostructured propellers. *Nano Lett*. 2009;9(6):2243–5.
- [208] Mahoney AW, et al. Velocity control with gravity compensation for magnetic helical microswimmers. *Adv Robot*. 2011;25(8):1007–28.
- [209] Zeeshan MA, et al. Hybrid helical magnetic microrobots obtained by 3D template-assisted electrodeposition. *Small*. 2014;10(7):1284–8.
- [210] Wang X, et al. 3D printed enzymatically biodegradable soft helical microswimmers. *Adv Funct Mater*. 2018;28(45):1804107.
- [211] Huang H-W, et al. Adaptive locomotion of artificial microswimmers. *Sci Adv*. 2019;5(1):eaau1532.
- [212] Shi X, et al. A strain-engineered Helical structure as a self-adaptive magnetic microswimmer. *Chem NanoMat*. 2021.
- [213] Gauger E, Stark H. Numerical study of a microscopic artificial swimmer. *Phys Rev E*. 2006;74(2):021907.
- [214] Maier AM, et al. Magnetic propulsion of microswimmers with DNA-based flagellar bundles. *Nano Lett*. 2016;16(2):906–10.
- [215] Dolev A, Kaynak M, Sakar MS. On-board mechanical control systems for untethered microrobots. *Adv Intell Syst*. 2021;2000233.
- [216] Tam D, Hosoi A. Optimal feeding and swimming gaits of biflagellated organisms. *Proc Natl Acad Sci*. 2011;108(3):1001–6.

- [217] Kurtuldu H, et al. Flagellar waveform dynamics of freely swimming algal cells. *Phys Rev E*. 2013;88(1):013015.
- [218] Hu J, et al. Modelling the mechanics and hydrodynamics of swimming *E. coli*. *Soft matter*. 2015;11(40):7867–76.
- [219] Berti L, et al. Shapes enhancing the propulsion of multiflagellated helical microswimmers. 2021. arXiv preprint [arXiv:2103.05637](https://arxiv.org/abs/2103.05637).
- [220] Beyrand N, et al. Multi-flagella helical microswimmers for multiscale cargo transport and reversible targeted binding. In: 2015 IEEE/RSJ international conference on intelligent robots and systems (IROS). 2015. IEEE.
- [221] Quispe J, Régnier S. Magnetic miniature swimmers with multiple rigid flagella. In: 2020 IEEE international conference on robotics and automation (ICRA). 2020. IEEE.
- [222] Wolgemuth CW, Igoshin O, Oster G. The motility of mollicutes. *Biophys J*. 2003;85(2):828–42.
- [223] Williamson DL, Tully JG, Whitcomb RF. The genus *Spiroplasma* The mycoplasmas. 2012;71–112.
- [224] Balaramraja VS, et al. Modelling the undulation patterns of flying snakes. In: 2016 International conference on advances in computing, communications and informatics (ICACCI). 2016. IEEE.
- [225] Leoni M, et al. A basic swimmer at low Reynolds number. *Soft Matter*. 2009;5(2):472–6.
- [226] Tam D, Hosoi AE. Optimal stroke patterns for Purcell’s three-link swimmer. *Phys Rev Lett*. 2007;98(6):068105.
- [227] Passov E, Or Y. Dynamics of Purcell’s three-link microswimmer with a passive elastic tail. *Eur Phys J E*. 2012;35(8):1–9.
- [228] Wiesel O, Or Y. Optimization and small-amplitude analysis of Purcell’s three-link microswimmer model. *Proc R Soc A Math Phys Eng Sci*. 2016;472(2192):20160425.
- [229] Grover J, et al. Geometric motion planning for a three-link swimmer in a three-dimensional low Reynolds-number regime. In: 2018 annual american control conference (ACC). 2018. IEEE.
- [230] Alouges F, et al. Can magnetic multilayers propel artificial microswimmers mimicking sperm cells? *Soft Robot*. 2015;2(3):117–28.
- [231] Alouges F, et al. Energy-optimal strokes for multi-link microswimmers: Purcell’s loops and Taylor’s waves reconciled. *New J Phys*. 2019;21(4):043050.
- [232] Moreau C, Giraldi L, Gadêlha H. The asymptotic coarse-graining formulation of slender-rods, bio-filaments and flagella. *J R Soc Interface*. 2018;15(144):20180235.
- [233] Dowell E, McHugh K. Equations of motion for an inextensible beam undergoing large deflections. *J Appl Mech*. 2016;83(5):051007. <https://doi.org/10.1115/1.4032795>.
- [234] Kumar CS, Mohammad F. Magnetic nanomaterials for hyperthermia-based therapy and controlled drug delivery. *Adv Drug Deliv Rev*. 2011;63(9):789–808.